

Supporting Information

**Synergistic O₃ + OH Oxidation Pathway to Extremely Low-Volatility Dimers
Revealed in β -Pinene Secondary Organic Aerosol**

Christopher M. Kenseth^a, Yuanlong Huang^b, Ran Zhao^a, Nathan F. Dalleska^b,
J. Caleb Hethcox^a, Brian M. Stoltz^a, and John H. Seinfeld^{a,c,1}

^aDivision of Chemistry and Chemical Engineering, California Institute of Technology,
Pasadena, CA 91125

^bDivision of Geological and Planetary Sciences, California Institute of Technology,
Pasadena, CA 91125

^cDivision of Engineering and Applied Science, California Institute of Technology,
Pasadena, CA 91125

¹To whom correspondence should be addressed. E-mail: seinfeld@caltech.edu

Table of Contents

S1. Secondary Organic Aerosol (SOA) Formation Experiments	S3
S1.1 Caltech dual 24 m ³ Teflon Environmental Chambers (CTEC)	S3
S1.2 Caltech Photooxidation Flow Tube (CPOT)	S4
S2. Gas-Phase Measurements	S5
S3. Particle-Phase Measurements.....	S6
S3.1 Scanning Mobility Particle Sizer (SMPS)	S6
S3.2 High-Resolution Time-of-Flight Aerosol Mass Spectrometer (HR-ToF-AMS)	S7
S3.3 Particle-Into-Liquid Sampler (PILS)	S8
S3.4 Teflon Filter Samples	S8
S3.5 Ultra-Performance Liquid Chromatography/Negative Electrospray Ionization Quadrupole Time-of-Flight Mass Spectrometry [UPLC/(-)ESI-Q-TOF-MS].....	S9
S3.6 Hydrogen/Deuterium Exchange (HDX) UPLC/(-)ESI-Q-TOF-MS.....	S10
S3.7 Iodometry-Assisted UPLC/(-)ESI-Q-TOF-MS	S11
S4. Master Chemical Mechanism (MCM) Simulations.....	S13
S5. Synthesis of ¹³C-β-Pinene	S14
S6. Dimer Esters from Synergistic O₃ + OH Oxidation	S15
S6.1 Structure Elucidation	S15
S6.2 Heterogeneous Formation Mechanism	S17
S7. Quantification of SOA Molecular Constituents.....	S18
S7.1 Determination of (-)ESI Efficiency	S19
S7.2 Uncertainty Analysis	S23
S8. General Applicability of O₃ + OH Oxidation to Monoterpene SOA Formation	S24
References.....	S25
Figures (S1–S12)	S31
Tables (S1–S5).....	S38

S1. Secondary Organic Aerosol (SOA) Formation Experiments

Ozonolysis and photooxidation experiments were conducted in the Caltech dual 24 m³ Teflon Environmental Chambers (CTEC) (1, 2) and Caltech Photooxidation Flow Tube (CPOT) (3) at ambient temperature (~295 K) and atmospheric pressure (~1 atm). All experiments were carried out under dry conditions (<10% RH), in the presence of ammonium sulfate [(NH₄)₂SO₄] seed aerosol, and at mixing ratios of NO_x typical of the pristine atmosphere (<0.5 ppb). Experimental conditions are reported in Table S1.

S1.1 Caltech dual 24 m³ Teflon Environmental Chambers (CTEC)

Experiments in the CTEC were performed to examine the identity, abundance, and kinetics of molecular products in secondary organic aerosol (SOA) formed from the O₃- and OH-initiated oxidation of β -pinene. Prior to each experiment, the chamber was flushed with dry, purified air for 24 h such that the particle number and volume concentrations were less than 10 cm⁻³ and 0.01 μ m³ cm⁻³, respectively. β -pinene (~120 ppb) was added to the chamber by passing dry, purified air at 5 L min⁻¹ through a glass cylinder, heated to 50 °C in a water bath, containing a volumetric injection of liquid β -pinene (20 μ L, \geq 99%, Sigma-Aldrich) for 30 min. Polydisperse seed aerosol (~70 μ m³ cm⁻³, $\bar{D}_p \approx 95$ nm) was generated via atomization of a dilute (0.06 M) aqueous solution of (NH₄)₂SO₄ (Macron Fine Chemicals), followed by diffusive drying and neutralization. In select experiments, seed aerosol was produced from dilute aqueous solutions of (NH₄)₂SO₄ (0.02 M) and *cis*-pinic acid (Sigma-Aldrich) in 1:1 (~120 μ m³ cm⁻³, $\bar{D}_p \approx 130$ nm) and 2:1 (~140 μ m³ cm⁻³, $\bar{D}_p \approx 120$ nm) mass ratios.

For ozonolysis experiments, O₃ (~200 ppb) was produced via photolysis of O₂ by flowing dry, purified air at 5 L min⁻¹ through a custom-built UV O₃ generator for ~40 min. Ozonolysis experiments were conducted in the absence of an OH scavenger, resulting in an initial OH molar yield of 28–44% (4, 5). For photooxidation experiments, H₂O₂ provided the source of OH on photolysis under broadband UV irradiation (blacklight spectrum centered at 350 nm). H₂O₂ (280 μ L, 50% w/w in H₂O, Sigma-Aldrich) was introduced into the chamber from a glass bulb, heated to 40 °C in a water bath, over a 1-h period with a flow of dry, purified air at 5 L min⁻¹, resulting in an initial H₂O₂ mixing ratio of ~4 ppm. At these relatively high mixing ratios of H₂O₂, significant

levels of HO₂ are produced via the OH + H₂O₂ reaction, which is favored at the slow chamber photolysis rate of H₂O₂. The steady-state concentrations of OH and HO₂ in these experiments were $\sim 2 \times 10^6$ and $\sim 1 \times 10^{10}$ molecules cm⁻³, respectively, as determined in a previous study (6). The duration of both ozonolysis and photooxidation experiments was ~ 4 h. Under these conditions, $\sim 70\%$ of the injected β -pinene was consumed in each experiment.

S1.2 Caltech Photooxidation Flow Tube (CPOT)

Due to its steady-state operating conditions, the CPOT was utilized to collect sufficient quantities of β -pinene SOA mass for detailed molecular-level composition and structural analysis by offline mass spectrometric and chromatographic techniques. An in-depth description of the CPOT and its standard operating protocol is presented elsewhere (3). Briefly, the CPOT consists of two 1.2 m \times 17 cm i.d. cylindrical quartz tubes, surrounded by an external water jacket and flanged together with clamps and chemically resistant O-rings. Reactants are thoroughly mixed at the inlet to the reactor in a stainless steel static mixer prior to passage through a conical diffuser that serves to expand the mixed flow to the diameter of the cylindrical section while maintaining an idealized laminar profile. A transition cone at the end of the reactor concentrates gas/particle-phase products into a common sampling line that can be split among multiple instruments. Samples extracted at the end of the reactor thus represent so-called cup-mixed averages of the entire reactor cross section. The total flow rate through the CPOT is 12.5 L min⁻¹, giving rise to an average residence time of 3.5 min. The Reynolds number (Re) in the cylindrical section of the reactor at this flow rate is ~ 125 , indicating laminar flow ($Re < 2100$).

β -pinene was introduced into the CPOT by passing dry, purified air at 500 mL min⁻¹ through a glass cylinder into which liquid β -pinene ($\geq 99\%$, Sigma-Aldrich) was continuously injected from a gas-tight volumetric syringe at 0.702 μ L h⁻¹ using a single syringe infusion pump (11 Plus, Harvard Apparatus), resulting in a steady-state β -pinene mixing ratio of ~ 150 ppb. Polydisperse seed aerosol ($\sim 75 \mu\text{m}^3 \text{ cm}^{-3}$, $\bar{D}_p \approx 85$ nm) was generated via continuous atomization of a dilute (0.01 M) aqueous solution of (NH₄)₂SO₄ (Macron Fine Chemicals), followed by diffusive drying and neutralization. A steady-state mixing ratio of O₃ of ~ 1 ppm was produced via photolysis of O₂ by flowing dry, purified air at 100 mL min⁻¹ through a custom-built UV O₃ generator. Ozonolysis

experiments were carried out both in the presence and absence of scavengers for OH and stabilized Criegee intermediates (SCIs). Cyclohexane ($\geq 99\%$, Fisher Scientific) was employed as an OH scavenger (Fig. 2), while ultra-pure water (18 M Ω , <3 ppb TOC, Millipore Milli-Q) and formic acid (98%, Fluka) were utilized as SCI scavengers (Fig. S1). For experiments featuring either cyclohexane or formic acid, steady-state mixing ratios of ~ 25 and 15 ppm, respectively, were achieved by passing a flow of dry, purified air at 500 mL min $^{-1}$ over the surface of a reservoir of the liquid reagent (i.e., a Stefan tube) (7). For experiments performed under humid conditions, dry, purified air at 15 L min $^{-1}$ was bubbled through a water reservoir to produce a steady-state water vapor mixing ratio in the CPOT of 1% (i.e., 43% RH).

Given recommended k_{OH} values for cyclohexane and β -pinene of 7.2×10^{-12} (8) and 7.89×10^{-11} cm 3 molecules $^{-1}$ s $^{-1}$ (9), respectively, the OH scavenging efficiency of the added cyclohexane was 93.5%. As rate coefficients for bimolecular reactions of the C $_9$ β -pinene SCIs are unknown, an estimated $k_{\text{SCI}+\text{HCOOH}}$ value of 1.7×10^{-12} cm 3 molecules $^{-1}$ s $^{-1}$ for α -pinene (10) was adopted as a surrogate for reaction with both formic acid and the carbonyls/organic acids formed from β -pinene ozonolysis, given that reactions of SCIs with organic acids are far more rapid than reactions with carbonyls (11). Likewise, $k_{\text{SCI}+\text{H}_2\text{O}}$ and $k_{\text{SCI}+(\text{H}_2\text{O})_2}$ values of 4.0×10^{-17} and 7.0×10^{-13} cm 3 molecules $^{-1}$ s $^{-1}$, respectively, predicted for (CH $_3$) $_2$ COO (12) were adopted for reaction of the C $_9$ β -pinene SCIs with water and the water dimer. Accordingly, assuming complete conversion of β -pinene to reactive carbonyls/organic acids (should clearly be lower) and a water dimer concentration equal to 0.06% that of the monomer (13), the minimum SCI scavenging efficiencies of the added formic acid and water vapor were 99.1 and 94.5%, respectively.

S2. Gas-Phase Measurements

β -pinene mixing ratios were quantified with an Agilent 6890N gas chromatograph equipped with a flame ionization detector (GC/FID) and operated with an Agilent HP-5 column (30 m \times 0.32 mm, 0.25 μ m). The GC/FID was calibrated with a commercial β -pinene standard ($\geq 99\%$, Sigma-Aldrich) over a mixing ratio range from 100 to 200 ppb using a gas-tight volumetric syringe and a mass-controlled dilution flow of N $_2$ into a 100 L Teflon bag. The GC/FID was also calibrated with ppm-level bags (10–20 ppm) prepared via an analogous method and cross-calibrated using Fourier

transform infrared spectroscopy (FT-IR) with tabulated absorption cross sections for β -pinene (25). O_3 and NO_x mixing ratios were quantified by a Horiba APOA-360 O_3 absorption monitor and a Teledyne T200 NO_x monitor, respectively. The detection limits for O_3 , NO , and NO_2 are 0.5, 0.4, and 0.4 ppb, respectively. Temperature and RH were monitored in the CTEC with a Vaisala HMM211 probe and in the CPOT with an Omega RH-USB sensor.

S3. Particle-Phase Measurements

S3.1 Scanning Mobility Particle Sizer (SMPS)

Aerosol size distributions and number concentrations for D_p between ~ 15 and 800 nm were measured with a custom-built scanning mobility particle sizer (SMPS) consisting of a TSI 3081 differential mobility analyzer (DMA) coupled to a TSI 3010 condensation particle counter (CPC). The DMA is operated in a closed-system configuration with a recirculating sheath and excess flow of 2.67 L min^{-1} and an aerosol flow of 0.515 L min^{-1} . The column voltage is scanned from 15 to 9850 V over a 4-min interval. A more detailed overview of the SMPS operation is provided elsewhere (2). For β -pinene SOA formation experiments performed in this study, the initial $(NH_4)_2SO_4$ seed volume was $\sim 60\text{--}80 \text{ }\mu\text{m}^3 \text{ cm}^{-3}$, with \bar{D}_p of $\sim 80\text{--}100$ nm and a size distribution spanning from ~ 20 to 600 nm. As a result of particle growth driven by gas/particle-phase chemistry and gas-particle partitioning, \bar{D}_p shifted to ~ 150 nm in steady-state CPOT experiments and to ~ 230 nm after ~ 4 h of reaction in CTEC experiments.

Aerosol volume concentrations were calculated assuming homogeneous spherical particles. To enable direct comparison with the concentrations of individual molecular products detected in suspended SOA using offline mass spectrometry, corrections for particle wall loss were neglected. Instead, suspended SOA volume concentrations were derived by applying an exponential fit to the decay of pure $(NH_4)_2SO_4$ seed and subtracting the extrapolated seed volume concentrations from the measured volume concentrations of total suspended aerosol (Fig. S2). SOA mass concentrations were calculated assuming an effective density for β -pinene SOA of 1.25 g mL^{-1} (26–29). Growth profiles of suspended SOA produced from the O_3 - and OH-initiated oxidation of β -pinene over ~ 4 h of reaction in the CTEC are shown in Fig. S3A.

The maximum suspended SOA mass loadings achieved during β -pinene ozonolysis and photooxidation experiments over ~ 4 h of reaction in the CTEC (Table S1, Exps. 1 and 2) were 35 and $54 \mu\text{g m}^{-3}$, respectively (Fig. S3A). These mass loadings are within a factor of 2 to 10 of ambient organic aerosol (OA) mass concentrations recently measured in forested regions dominated by monoterpene emissions: $1.9\text{--}6.8 \mu\text{g m}^{-3}$ (K-puszt, Hungary; BIOSOL 2006) (30), $4.3 \pm 2.3 \mu\text{g m}^{-3}$ (Sierra Nevada Mountains; BEARPEX 2009) (31), $<1\text{--}23 \mu\text{g m}^{-3}$ (SMEAR II Station, Hyytiälä, Finland; HUMPPA-COPEC 2010) (32), $2.9\text{--}5.3 \mu\text{g m}^{-3}$ (SMEAR II Station, Hyytiälä, Finland) (33), and $4.8 \mu\text{g m}^{-3}$ (Centreville, Alabama; SOAS 2013) (34). Consequently, the mass loadings of β -pinene SOA generated in this study, and in turn the molecular composition, can be considered relevant to the real atmosphere.

S3.2 High-Resolution Time-of-Flight Aerosol Mass Spectrometer (HR-ToF-AMS)

Submicrometer, nonrefractory aerosol chemical composition was quantified with an Aerodyne high-resolution time-of-flight aerosol mass spectrometer (HR-ToF-AMS), providing chemical speciation of sulfate, ammonium, and organic constituents at a frequency of 0.1 Hz. The working principles and modes of operation of the HR-ToF-AMS are described in detail elsewhere (35). Briefly, submicrometer aerosol ($35 \text{ nm--}1.5 \mu\text{m}$) is sampled into the instrument through an aerodynamic lens at a flow rate of $\sim 1.3 \text{ mL s}^{-1}$, producing a collimated particle beam that is directed onto a resistively heated surface where particles undergo vaporization ($\sim 600^\circ\text{C}$) and electron impact (EI) ionization (70 eV). The resulting ions are detected with a custom-designed ToFwerk HR-ToF-MS configured in V-mode. Data were analyzed using the SQUIRREL v1.59B and PIKA v1.19B modules for Igor Pro v7.02 (WaveMetrics), and were corrected for gas-phase interferences (36, 37) and composition-dependent collection efficiencies (38). Detection limits for each class of chemical constituents were calculated as three times the standard deviation of blank signals ($3\sigma_{\text{blank}}$) measured from high-efficiency particulate arrestance (HEPA) filter samples taken before each experiment. The instrumental ionization efficiency was calibrated using dry, 350 nm ammonium nitrate (NH_4NO_3) particles, generated via atomization of a dilute (0.01 M) aqueous solution of NH_4NO_3 (Macron Fine Chemicals) and size-selected with a DMA. Elemental O:C and H:C ratios, as well as average carbon oxidation states ($\overline{\text{OS}}_{\text{C}} = 2 \text{ O:C} - \text{H:C}$), of β -pinene SOA were calculated using the “Improved-Ambient” elemental analysis method for AMS spectra (39). After

~4 h of reaction in the CTEC, O:C, H:C, and $\overline{\text{OS}}_{\text{C}}$ values for O₃-derived β -pinene SOA were found to be 0.38, 1.64, and -0.88, respectively, whereas for OH-derived β -pinene SOA respective values of 0.35, 1.75, and -1.05 were obtained (Fig. S3B–D). These results are in good agreement with O:C and H:C ratios reported in previous laboratory studies for α -pinene SOA generated from ozonolysis (O:C = 0.30–0.43; H:C = 1.47–1.66) (23, 39–43) and photooxidation (O:C = 0.36–0.40; H:C = 1.60–1.71) (23, 44).

S3.3 Particle-Into-Liquid Sampler (PILS)

A custom-modified particle-into-liquid sampler (PILS) was used to collect chamber-generated β -pinene SOA for molecular-level characterization of particle-phase dynamics. A detailed description of the Caltech PILS, which is based on a modification of the original design of Weber et al. (45), is presented elsewhere (46). Briefly, chamber aerosol is sampled into the instrument through a 1 μm cut size impactor at a flow rate of 12.5 L min⁻¹ and passed successively through individual acid and base denuders and an organic carbon denuder to remove inorganic and organic vapors. A steam flow generated from ultra-pure water (18 M Ω , <3 ppb TOC, Millipore Milli-Q) at 100 °C is adiabatically mixed with the cooler aerosol flow in a condensation chamber, creating a water supersaturation environment in which particles grow sufficiently large ($D_p > 1 \mu\text{m}$) for collection by inertial impaction onto a quartz plate. Impacted particles are transported to a debubbler by a washing flow (0.15 mL min⁻¹) of ultra-pure water (18 M Ω , <3 ppb TOC, Millipore Milli-Q). The sampled liquid is delivered into vials held on a rotating carousel. Under the current configuration (5-min duty cycle), a total of 48 liquid samples were collected for CTEC experiments with ~4-h duration. Sample vials were stored at -16 °C immediately after collection. The PILS method is particularly suited to the collection of oxygenated, water-soluble organic carbon (WSOC), which typically accounts for a majority of SOA. The overall PILS collection efficiency for β -pinene SOA was estimated to be >85%, based on an empirical correlation of water solubility and the average O:C ratio of the aerosol ensemble derived from HR-ToF-AMS measurement (47).

S3.4 Teflon Filter Samples

β -pinene SOA from steady-state CPOT and select CTEC experiments was collected on Pall Life Sciences Teflon membrane disc filters (2 μm pore size, 47 mm diameter) at a sampling flow rate

of 10 L min^{-1} . Collection periods for CPOT experiments ranged from 15 to 24 h per filter sample, while during CTEC experiments filters were collected for 4 h. A cylindrical diffusion denuder packed with activated charcoal (Sigma-Aldrich) was placed upstream of the sampling apparatus to remove O_3 and gas-phase species, thereby preventing on-filter reactions and further partitioning of compounds from the gas phase to collected particles. The SOA particle loss through the denuder was assumed to be negligible (48). The mass of SOA collected on each filter was typically 2–3 mg for CPOT experiments and <1 mg for CTEC experiments. Filters were stored at -16°C immediately after collection.

Filter samples were extracted into 10 mL ultra-pure water ($18 \text{ M}\Omega$, <3 ppb TOC, Millipore Milli-Q) for 1 h using an orbital shaker at 200 rpm, as extraction via ultrasonic agitation has been shown to cause degradation of α -pinene SOA molecular markers (e.g., *cis*-pinic acid) as well as elevated concentrations of particle-bound peroxides, likely due to formation of OH radicals by acoustic cavitation that react with SOA constituents and combine to form H_2O_2 (49). To account for variations in filter collection and extraction efficiency, the total organic carbon (TOC) content of filter extracts was quantified using an OI-Analytical Aurora 1030W TOC Analyzer. The total carbon (TC) method was employed, wherein all carbon-containing species (i.e., organic and inorganic) are oxidized to CO_2 by sodium persulfate and phosphoric acid at 100°C and then detected by nondispersive IR spectroscopy. The TC content of blank filter extracts was used for background subtraction. A detection limit of 0.6 ppmC was calculated from the standard deviation of the TC content of the blank filter extracts ($3\sigma_{\text{blank}}$). The method was calibrated using standard solutions of potassium hydrogen phthalate ($\geq 99\%$, Sigma-Aldrich), and the accuracy of the method was verified to within 5% using solutions of *meso*-erythritol ($\geq 99\%$, Sigma-Aldrich) and D-sorbitol ($\geq 98\%$, Sigma-Aldrich) of known concentration.

S3.5 Ultra-Performance Liquid Chromatography/Negative Electrospray Ionization Quadrupole Time-of-Flight Mass Spectrometry [UPLC/(–)ESI-Q-TOF-MS]

β -pinene SOA filter extracts and PILS samples were analyzed by a Waters ACQUITY ultra-performance liquid chromatography (UPLC) I-Class system coupled to a Xevo G2-S quadrupole time-of-flight mass spectrometer (Q-TOF-MS) equipped with an electrospray ionization (ESI) source and operating at a mass resolution ($m/\Delta m$) of 20,000–34,000 and a mass accuracy of ≤ 5

mDa. An ACQUITY BEH C₁₈ column (1.7 μ m, 2.1 mm \times 50 mm) kept at 30 °C was used to separate SOA molecular constituents. The polar (A) and nonpolar (B) eluents were 0.1% v/v formic acid (98%, Fluka) in ultra-pure water (18 M Ω , <3 ppb TOC, Millipore Milli-Q) and 100% acetonitrile (OptimaTM LC/MS, Fisher Scientific), respectively. The 12-min eluent program was: (0–2.0 min) 99% A and 1% B; (2.0–10.0 min) linear gradient to 10% A and 90% B; (10.0–10.2 min) 10% A and 90% B; (10.2–10.5 min) linear gradient to 99% A and 1% B; (10.5–12 min) 99% A and 1% B. The total flow rate was 0.3 mL min⁻¹ and the injection volume was 10 μ L. The sample temperature was 4 °C. Optimized ESI conditions were: 2.0 kV capillary voltage, 40 V sampling cone, 80 V source offset, 120 °C source temperature, 400 °C desolvation temperature, 30 L h⁻¹ cone gas flow, and 650 L h⁻¹ desolvation gas flow.

Negative (–) ion mass spectra were acquired from m/z 40 to 1000, following calibration using sodium formate clusters ([Na_x(HCOO)_{x+1}][–]) prepared from formic acid (98%, Fluka) and sodium hydroxide (50% w/w in H₂O, Fisher Scientific). All analytes were detected as pseudomolecular [M–H][–] ions, generated via deprotonation of parent molecules during (–)ESI. The calibrated mass axis was locked to the [M–H][–] ion of a lock spray of leucine enkephalin (\geq 95%, AnaSpec) at m/z 554.2615. MS/MS spectra were collected in tandem with MS measurements (50% duty cycle) via collision-induced dissociation (CID; Ar collision gas) of parent ions, quadrupole-selected with an isolation width of 3 Da during specified retention time (RT) ranges, using a collision energy ramping program (15–50 V). Instrumental stability (i.e., chromatographic and mass spectral reproducibility) was verified to within 3% using a standard solution of adipic acid (99%, Sigma-Aldrich) and *cis*-pinonic acid (98%, Sigma-Aldrich) run periodically (one standard every 10 samples) during routine analysis. Data were acquired and processed using MassLynx v4.1 software. Molecular formulas (C_xH_yO_z) of parent and fragment ions in MS and MS/MS spectra were assigned with mass tolerances of <7 ppm and supported by the associated ¹³C isotope distributions.

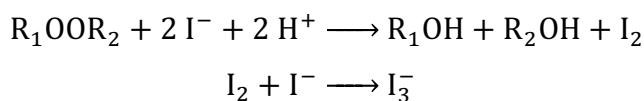
S3.6 Hydrogen/Deuterium Exchange (HDX) UPLC/(–)ESI-Q-TOF-MS

β -pinene SOA filters from steady-state CPOT experiments were extracted into 10 mL D₂O (99.9 atom % D, Sigma-Aldrich) for 1 h with an orbital shaker at 200 rpm and analyzed via

UPLC/(–)ESI-Q-TOF-MS using 0.1% v/v formic acid (98%, Fluka) in D₂O as the polar eluent. This approach facilitated deuterium substitution (H→D) of labile hydrogens in the SOA constituents while preserving chromatographic separation, enabling quantification of the number of exchangeable hydrogens in the structures of the identified monomers and dimers based on systematic shifts in *m/z* (Table 1). The *m/z* of each SOA constituent shifted by one mass unit for every exchangeable hydrogen present in the molecule in addition to the site deprotonated to form the [M–H][–] ion. For most analytes, H/D exchange proceeded to completion (Fig. S4A and C), indicative of structures containing only fairly acidic and easily exchangeable hydrogens (i.e., –OH, –OOH, and –COOH). However, for certain dimeric compounds, *m/z* 355 (C₁₈H₂₈O₇; RT 6.24), *m/z* 373 (C₁₈H₃₀O₈; RT 5.99), *m/z* 369 (C₁₉H₃₀O₇; RT 6.48), *m/z* 353 (C₁₉H₃₀O₆; RT 6.15), and *m/z* 355 (C₁₈H₂₈O₇; RT 5.27), only partial H/D exchange was observed (Fig. S4B), suggesting that the structures of these dimers contain moderately acidic hydrogens, such as α hydrogens adjacent to carbonyls. As p*K*_a values for aldehyde α hydrogens are typically comparable to those of alcohols (~17) whereas p*K*_a values of ketone α hydrogens are generally much higher (~20) (50), aldehyde functionalities are assumed to be responsible for the partial H/D exchange exhibited by the specified dimers. Interestingly, partial H/D exchange of the α hydrogens of β-dicarbonyls, which are significantly more acidic (p*K*_a ≈ 9–14) than those of aldehydes (50), was recently observed via ¹H NMR spectroscopy (51), providing indirect support for the partial H/D exchange hypothesized for aldehyde α hydrogens.

S3.7 Iodometry-Assisted UPLC/(–)ESI-Q-TOF-MS

Conventional iodometry was coupled to UPLC/(–)ESI-Q-TOF-MS, as described by Zhao et al. (52), to identify organic peroxides [i.e., hydroperoxides (ROOH) and organic peroxides (ROOR)] at the molecular level in β-pinene SOA. In the presence of an acid catalyst, I[–] selectively reduces organic peroxides to the corresponding alcohol, liberating I₂ and subsequently forming I₃[–] in solutions of excess I[–]:



As the iodometric method has been shown to have negligible impact on species that do not possess peroxide functionalities, comparison of treated and control samples via UPLC/(–)ESI-Q-TOF-MS enables identification of peroxide-containing species based on the disappearance of signals corresponding to detected molecular constituents.

Samples were prepared by acidifying an SOA filter extract to pH 2 with formic acid (50% w/w in H₂O, Fluka). To an aliquot of the acidified extract, a concentrated aqueous solution of potassium iodide (KI, 99%, Sigma-Aldrich), made fresh daily and purged with N₂, was added such that the concentration of I[–] was 60 mM. As a control, a second aliquot was diluted to the final volume of the treated sample with ultra-pure water (18 MΩ, <3 ppb TOC, Millipore Milli-Q). In this way, differences between treated and control samples reflected only changes induced by iodometry and not differences due to dilution or acidification. Immediately following dilution or KI addition, the treated and control samples were purged with N₂ and placed in air-tight vials in the dark for 7 h prior to analysis by UPLC/(–)ESI-Q-TOF-MS to ensure completion of the iodometric reaction. The iodometric method was validated against a series of H₂O₂ (50% w/w in H₂O, Sigma-Aldrich) solutions of known concentration.

The abundances of the 23 identified dimers (Table 1) did not change significantly (<15%) in response to iodometry (Fig. S5), indicating that these compounds do not contain ROOH or ROOR functionalities. Although somewhat surprising, given that organic peroxides have been found to account for a significant mass fraction (12–85%) of SOA derived from monoterpene oxidation (53–57), the absence of (hydro)peroxide groups in the dimer structures is not unreasonable. We recently demonstrated using iodometry-assisted UPLC/(–)ESI-Q-TOF-MS that dimers detected in α-pinene SOA also lack ROOH and ROOR moieties, despite conventional spectrophotometric iodometry suggesting that ~15% of the α-pinene SOA mass is attributable to organic peroxides (52).

These findings are consistent with the decomposition of particle-bound organic peroxides, likely to smaller peroxides that cannot be detected by UPLC/(–)ESI-Q-TOF-MS but can contribute to the total peroxide content quantified via spectrophotometric iodometry. The labile nature of

organic peroxides in biogenic SOA has been demonstrated in a number of recent studies (57–59), with reported decomposition timescales on the order of a few hours. Formation of OH radicals (60) and H₂O₂ (61, 62) from aqueous-phase monoterpene SOA (e.g., filter extracts and PILS samples) has also been observed, indicative of peroxide decomposition or hydrolysis. In addition, decomposition of multifunctional organic peroxides (e.g., peroxyhemiacetals and diacyl peroxides) can lead to nonperoxide species, including carboxylic acids, aldehydes, alcohols, and esters (21, 53).

S4. Master Chemical Mechanism (MCM) Simulations

The Master Chemical Mechanism version 3.2 (MCMv3.2) (54, 63) was used to predict the time-dependent concentrations of OH, HO₂, and RO₂ during β -pinene ozonolysis in the CTEC, as well as the fractions of β -pinene that react with O₃ vs. OH. The initial conditions for the simulations were those from Exp. 1 in Table S1 (i.e., 123 ppb β -pinene, 200 ppb O₃, zero NO_x, 295 K, 1 atm, and 5% RH). Three variations of the gas-phase β -pinene ozonolysis mechanism were implemented: (i) MCMv3.2 without modification, (ii) MCMv3.2 revised with the theoretical first-generation ozonolysis branching ratios from Fig. 6 in Nguyen, Peeters, and Vereecken (5) (MCMv3.2 + NPV), and (iii) the mechanism from (ii) further modified with the theoretical β -pinene photooxidation mechanism of Vereecken and Peeters (64) (MCMv3.2 + NPV + VP). Key areas in which these theoretical mechanisms, based on quantum chemical calculations and statistical kinetic analysis, deviate from the oxidation schemes currently incorporated in MCMv3.2 are discussed in detail in the corresponding references.

The observed first-order decay of β -pinene is well replicated by each of the three ozonolysis mechanisms; the two modified mechanisms produce slightly better agreement (Fig. S6A). The simulated concentration profiles of OH and RO₂ appear to be fairly insensitive to the gas-phase ozonolysis mechanism employed, yielding concentrations of $\sim 1.5 \times 10^5$ and $\sim 2.0 \times 10^{10}$ molecules cm⁻³, respectively, after 4 h of reaction (Fig. S6B). Conversely, HO₂ profiles differ moderately between the three oxidation schemes, with concentrations after 4 h ranging from ~ 1.5 to 3.0×10^7 molecules cm⁻³. Based on these simulations, OH-initiated oxidation accounts for $\sim 20\%$ of the β -pinene consumption over a 4-h ozonolysis experiment. Assuming typical $k_{\text{RO}_2+\text{RO}_2}$ and

$k_{\text{RO}_2+\text{HO}_2}$ values of 6.7×10^{-13} and $2.09 \times 10^{-11} \text{ cm}^3 \text{ molecules}^{-1} \text{ s}^{-1}$, respectively (65), the simulated RO_2 and HO_2 concentration profiles suggest that $\text{RO}_2 + \text{HO}_2$ chemistry is of minor significance to the formation of molecular products in SOA derived from β -pinene ozonolysis in the CTEC.

S5. Synthesis of ^{13}C - β -Pinene

Unless otherwise stated, reactions were performed in flame-dried glassware under an Ar or N_2 atmosphere using dry, deoxygenated solvents. Solvents were dried by passage through an activated alumina column under Ar. Chemicals and reagents were purchased from Sigma-Aldrich and used as received. Reaction temperatures were controlled by an IKA Mag temperature modulator. Thin-layer chromatography (TLC) was performed using E. Merck silica gel 60 F254 precoated plates (0.25 mm) and visualized by UV fluorescence quenching, potassium permanganate staining, or *p*-anisaldehyde staining. SiliaFlash P60 Academic Silica gel (particle size 0.040–0.063 mm) was used for flash column chromatography. ^1H NMR spectra were recorded on a Bruker AVANCE HD 400 MHz NMR spectrometer and are reported in terms of chemical shift relative to residual CHCl_3 (δ 7.26 ppm). Data for ^1H NMR are reported as follows: chemical shift (δ ppm) (multiplicity, coupling constant, integration). Abbreviations are used as follows: s = singlet, d = doublet, t = triplet, m = multiplet. Reported spectra include minor solvent impurities of ether (δ 3.48, 1.21) and petroleum ether (δ 1.26, 0.86), which do not impact product assignments. High-resolution mass spectra were obtained using a Waters GCT Premier TOF-MS operating in EI ionization mode at a mass resolution ($m/\Delta m$) of 7000, interfaced with an Agilent 6890 GC with electronic pressure control and a split-splitless inlet. The GC was equipped with a Phenomenex ZB-5MS column (30 m \times 0.25 mm, 0.25 μm) and operated in split mode at a split ratio of 240:1. The TOF-MS was calibrated from m/z 40 to 614 using perfluorotributylamine (PFTBA, Sigma-Aldrich) as a mass reference compound. The calibrated mass axis was locked to the $(\text{CF}_2)_3\text{CF}_3^+$ ion at m/z 218.985.

^{13}C - β -Pinene. Triphenylphosphine (4.59 g, 17.5 mmol) was added to a solution of ^{13}C -iodomethane (2.5 g, 17.5 mmol) in benzene (15 mL) and the reaction was stirred for 72 h. The reaction was filtered, washing with benzene, and the filtrate was dried under reduced pressure to provide methyl- ^{13}C -triphenylphosphonium iodide in quantitative yield as a white solid. *n*-Butyllithium (2.5 M, 1.7 mL, 4.33 mmol) was added to a suspension of methyl- ^{13}C -

triphenylphosphonium iodide (1.86 g, 4.63 mmol) in THF (8 mL) at 0 °C and was stirred for 30 min. Nopinone (0.400 g, 2.89 mmol) was added and the reaction was heated under reflux for 18 h. The reaction was allowed to cool to room temperature (25 °C), diluted with petroleum ether, filtered through celite, and concentrated under reduced pressure. The crude reaction mixture was purified via flash column chromatography, eluting with petroleum ether to provide 0.300 g of ¹³C-β-Pinene as a mixture (1:1) with petroleum ether (Scheme 1). Note that due to the volatile nature of the product, the pure material was not fully concentrated. However, the residual petroleum ether affects neither product assignment nor subsequent experiments. ¹H NMR (300 MHz, CDCl₃) δ 4.85 (d, *J* = 20.2 Hz, 1 H), 4.33 (d, *J* = 22.0 Hz, 1 H), 2.66–2.39 (m, 2 H), 2.38–2.15 (m, 2 H), 1.97 (tt, *J* = 5.8, 3.0 Hz, 1 H), 1.94–1.77 (m, 2 H), 1.42 (d, *J* = 9.8 Hz, 1 H), 1.24 (s, 3 H), 0.72 (s, 3 H) (Fig. S7). High-resolution mass spectra indicate ¹³C incorporation (Fig. S8).

S6. Dimer Esters from Synergistic O₃ + OH Oxidation

S6.1 Structure Elucidation

As discussed in the main text, MS/MS spectra of the ¹³C-labeled dimers and their ¹²C isotopologues revealed distinct OH-derived (¹³C-mass-shifted) and O₃-derived (unshifted) fragmentation patterns (Table S3). Detailed analysis of these spectra, constrained by HDX and iodometry-assisted UPLC/(–)ESI-Q-TOF-MS, particle-phase kinetic analysis, and the extant mechanisms of β-pinene ozonolysis and photooxidation, afforded insight into the structures of these dimeric compounds.

The O₃-derived fragmentation patterns in the MS/MS spectra (Fig. 3 and Table S3) of the dimer esters (Table 1, type 1) are comparable to those observed for three abundant terpenoic acids identified in β-pinene SOA: *m/z* 185 (C₉H₁₄O₄; RT 4.33), *m/z* 171 (C₈H₁₂O₄; RT 4.06), and *m/z* 189 (C₈H₁₄O₅; RT 3.32). Based on comparison with LC/(–)ESI-MS data reported in the literature (66, 67), these SOA products, and in turn the O₃-derived dimer ester precursors, are assigned to three well-characterized dicarboxylic acids: *cis*-pinic acid (C₉H₁₄O₄), *cis*-norpinic acid (C₈H₁₂O₄), and diaterpenylic acid (C₈H₁₄O₅). In the case of the compound at *m/z* 185, comparison of its chromatographic and mass spectrometric behavior with that of a commercial *cis*-pinic acid standard (Sigma-Aldrich) corroborated the assignment. The extracted ion chromatograms, MS spectra, MS/MS spectra, and proposed fragmentation pathways for the three dicarboxylic acids are

presented in Fig. S9. It is noted that there are differences between the relative abundances of the MS/MS fragment ions in Fig. S9 and those of the O₃-derived fragment ions of the dimer esters shown in Fig. 3. This feature can be rationalized by a difference in internal energy between the first- and second-generation dicarboxylic acid ions. Namely, the dicarboxylic acid ions produced via CID of dimer ester ions will have higher internal energy and undergo more extensive fragmentation on CID than those formed directly from (–)ESI. The strong correlation between the time-resolved particle-phase abundances of the dimer esters and their presumed dicarboxylic acid building blocks (Fig. 4A–C) further substantiates these structural assignments.

The OH-derived monomeric units are characterized by the ionic [M–H][–] formulas [C₁₀H_{15,17}O_{2–7}][–], indicative of OH addition to β-pinene (C₁₀H₁₆) followed by varying degrees of O₂ incorporation, isomerization, and bimolecular radical chemistry. As iodometry-assisted UPLC/(–)ESI-Q-TOF-MS demonstrated that the dimer esters do not contain ROOH functionalities, formation of OH-derived building blocks is assumed not to proceed via either RO₂ autoxidation (i.e., regenerative RO₂ formation following intramolecular H-shifts) (68, 69) or HO₂-mediated reaction channels. Simulations of HO₂ and RO₂ concentrations during β-pinene ozonolysis in the CTEC also suggest that RO₂ + HO₂ chemistry is not significant in dimer ester production (*SI Appendix*, S4). Tentative molecular structures for the OH-derived monomers, consistent with observed fragmentation patterns, are formulated based on the theoretical β-pinene photooxidation mechanism of Vereecken and Peeters (64), which derives from quantum chemical calculations, statistical kinetics, and structure-activity relationships (SARs). A key feature of this mechanism is the predicted accessibility of ring closure reactions of unsaturated RO and RO₂ radicals, which bring simulated nopinone and acetone yields in line with experimental data. Suggested OH-derived monomeric structures are constrained by the total number of exchangeable hydrogens in the structures of the dimer esters, quantified using HDX UPLC/(–)ESI-Q-TOF-MS, together with the known structures of the inferred O₃-derived dicarboxylic acids. Fragmentation pathways for the dimer esters with proposed OH-derived precursors (Table S4) are presented in Fig. S10. These pathways consist of established charge-retention and charge-migration fragmentations (e.g., remote hydrogen rearrangements and pericyclic reactions), and are based on fundamental organic reactivity and ion stability principles (70, 71). While at least two structural

isomers are possible for each proposed dimer ester, depending on the position of the ester linkage, only the structure and fragmentations of the most likely isomer are considered.

S6.2 Heterogeneous Formation Mechanism

The formation of the major dimer ester at m/z 337 ($C_{19}H_{30}O_5$) in β -pinene photooxidation experiments carried out with *cis*-pinic acid and $(NH_4)_2SO_4$ seed (Fig. 5) corroborates the indirect MS/MS (Fig. 3A) and kinetic (Fig. 4A) evidence for heterogeneous formation via reactive uptake of a gas-phase, OH-derived monomer/intermediate by particle-bound *cis*-pinic acid. A heterogeneous rather than purely particle-phase mechanism is also supported by the absence of stable products corresponding to the OH-derived dimer ester precursors [e.g., m/z 169 ($C_{10}H_{18}O_2$) for the dimer ester at m/z 337 (Table S3)] in SOA generated from β -pinene ozonolysis. The details of the mechanism forming the ester linkage are presently unclear. However, the observed increase in the abundances of the dimer esters (11–46%) under humid conditions (43% RH) (Fig. S1) argues against formation via conventional esterification (i.e., carboxylic acid + alcohol). These findings are in line with a recent theoretical study demonstrating that particle-phase esterification of α -pinene ozonolysis products is thermodynamically unfavorable (72).

To rule out the possibility of dimer formation through accretion of condensed monomers, either on the filter or during the extraction process, β -pinene SOA from OH-initiated oxidation in the CTEC with pure $(NH_4)_2SO_4$ seed was collected on a Teflon filter uniformly coated with ~ 0.5 mg of *cis*-pinic acid (Sigma-Aldrich). A clean Teflon filter was also collected in parallel as a control, such that the mass of SOA collected on each filter was approximately equivalent. The filters were stored at room temperature (25 °C) for 48 h following collection, then extracted into 10 mL ultra-pure water (18 M Ω , <3 ppb TOC, Millipore Milli-Q) as described in *SI Appendix*, S3.4. Filter extracts were left at room temperature for 72 h prior to analysis by UPLC/(–)ESI-Q-TOF-MS. As shown in Fig. S11, the dimer ester at m/z 337 was not observed in either SOA sample, demonstrating that the dimer esters are not artifacts of on-filter or aqueous-phase reactions.

The β -pinene photooxidation experiments performed with *cis*-pinic acid and $(NH_4)_2SO_4$ seed suggest that the hypothesized mechanism of heterogeneous dimer formation requires a sufficient particle-phase concentration of semivolatile dicarboxylic acids, which may be limited in the

ambient atmosphere by inefficient gas-particle partitioning. However, recent field measurements of gas-particle partitioning of tracers for biogenic oxidation indicate that the fraction of *cis*-pinic acid residing in the particle phase (F_p) in forested locations is 0.3–0.4 during the day and 0.6–0.8 at night (34, 73). As the saturation mass concentrations (C^*) of the dicarboxylic acids identified as dimer ester precursors (*cis*-pinic acid, *cis*-norpinic acid, and diaterpenylic acid) are all on the order of $10 \mu\text{g m}^{-3}$ (74), the findings for *cis*-pinic acid imply that pinene-derived dicarboxylic acids undergo efficient absorptive equilibrium gas-particle partitioning under ambient conditions and should thus be present in the particle phase in sufficient quantities to facilitate heterogeneous dimer formation.

S7. Quantification of SOA Molecular Constituents

Mass concentrations of individual organic compounds in chamber-generated β -pinene SOA collected by PILS and analyzed off-line by UPLC/(–)ESI-Q-TOF-MS were calculated from the following expression:

$$C = \frac{Q_l \cdot \rho_l \cdot DF \cdot R}{Q_s \cdot CE_{PILS} \cdot IE} \quad (\text{S1})$$

where C is the particle-phase mass concentration of the compound ($\mu\text{g m}^{-3}$), Q_s is the aerosol sampling flow rate (12.5 L min^{-1}), Q_l is the rate of the washing flow (0.15 mL min^{-1}), DF is the dilution factor that accounts for water vapor condensation on the PILS impaction plate (assumed to be 1.1) (46), ρ_l is the density of the collected PILS sample (assumed to be the density of the washing flow, 1.0 g mL^{-1}), CE_{PILS} is the overall PILS collection efficiency for β -pinene SOA (estimated to be 0.85) (47), R is the UPLC/(–)ESI-Q-TOF-MS response (i.e., chromatographic peak area) for the compound, and IE is the compound-specific (–)ESI efficiency (ppb^{-1}). From comparison of the resulting particle-phase mass concentrations to the SMPS-derived suspended SOA mass loading, mass fractions of identified molecular products in β -pinene SOA were determined.

S7.1 Determination of (–)ESI Efficiency

In the case of small molecules (<1000 Da), such as those analyzed in the current work, the ESI process is described by the ion evaporation model (IEM) (75). Prior separation of analytes from the complex SOA matrix via UPLC precludes potential ion-source artifacts (e.g., signal suppression and noncovalent clustering), ensuring the quantitative nature of the method. As authentic standards were not available, the (–)ESI efficiencies of the three similarly structured dicarboxylic acids implicated as dimer ester precursors (*cis*-pinic acid, *cis*-norpinic acid, and diaterpenylic acid) were quantified using commercially available *cis*-pinic acid (Sigma-Aldrich) as a surrogate. A 5-point calibration curve ($n = 3$) was generated from aqueous solutions of *cis*-pinic acid spanning a concentration range from 50 to 1000 ng mL^{–1} (ppb); a linear response ($R^2 > 0.999$) was observed. The detection limit for *cis*-pinic acid, calculated as three times the standard deviation of the blank ($3\sigma_{\text{blank}}$), was found to be 1.2 ppb. The concentrations of the dicarboxylic acids measured in the PILS samples fell well above this threshold, and well within the calibrated linear range of the instrument.

Due to a lack of authentic standards, (–)ESI efficiencies of oligomers in monoterpene SOA are typically quantified using commercially available terpenoic acids as surrogates (e.g., *cis*-pinonic acid and *cis*-pinic acid) (22, 23, 31, 76, 77). The same approach was applied here, using the measured (–)ESI efficiency of *cis*-pinic acid as a proxy for those of the dimeric compounds detected in β -pinene SOA formed from O₃-initiated oxidation. The (–)ESI efficiencies of the identified dimers were also estimated theoretically via a linear model ($R^2 = 0.83$) developed by Krueve et al. (78):

$$\log RIE = (1.04 \pm 0.34) + (2.23 \pm 0.34) \cdot \alpha - (0.51 \pm 0.04) \cdot WAPS \cdot 10^5 \quad (\text{S2})$$

where $\log RIE$ is the (–)ESI efficiency relative to benzoic acid on a logarithmic scale (i.e., $\log RIE_{\text{benzoic acid}} = 0$), α is the degree of ionization in solution (a function of analyte pK_a and solution pH), and $WAPS$ (weighted average positive sigma) is a parameter that quantifies the extent of charge delocalization in anions (i.e., the distribution of charge density across an ionic surface):

$$WAPS = \frac{\int_{\sigma=0}^{\infty} \sigma p(\sigma) d\sigma}{A \int_{\sigma=0}^{\infty} p(\sigma) d\sigma} \quad (S3)$$

where σ is the polarization charge density on the ion surface ($e \text{ \AA}^{-2}$), $p(\sigma)$ is the probability function of σ , and A is the surface area of the anion (\AA^2). The dependence of $\log RIE$ on α and $WAPS$ is in good agreement with current understanding of the (–)ESI process, as compounds that are more extensively dissociated in the LC mobile phase (higher α) will yield a higher concentration of anions in ESI droplets, while anions with more delocalized charge (lower $WAPS$) will interact more weakly with other molecules/ions in ESI droplets, exhibit lower solvation energy and a lower tendency for ion pairing (i.e., less attraction to polar solvent molecules as well as cations in the droplet interior), and thus partition more readily to and evaporate more easily from ESI droplet surfaces (78).

The conductor-like screening model for real solvents (COSMO-RS) (79, 80) implemented in the Amsterdam Density Functional (ADF 2017.108) molecular modeling suite (81) was used to generate the charge density distributions (i.e., σ profiles) required to derive $WAPS$ parameters, as well as calculate analyte pK_a values. Gas-phase molecular and anionic geometries were optimized at the TZP level using the Becke-Perdew (BP) generalized-gradient approximation (GGA) exchange-correlation functional and the scalar zeroth-order regular approximation (ZORA) relativistic Hamiltonian. Default “ADF combi2005” COSMO-RS parameters, which are optimized for ADF calculations, were employed (81). Representative σ profiles of the $[M-H]^-$ ions of *cis*-pinic acid and the major dimer ester at m/z 337 ($C_{19}H_{30}O_5$) are shown in Fig. S12. The computed σ profiles, together with anionic surface areas, were used to evaluate $WAPS$ parameters. $WAPS$ values above 4.5×10^{-5} have been proposed to indicate anions with localized charge (82).

Aqueous pK_a values for each analyte were calculated from their free energies of dissociation in water (ΔG_{diss}), computed using the COSMO-RS continuum solvation model. Negligible differences in zero-point energy between the neutral and deprotonated forms of each analyte were assumed. Following the approach of Eckert et al. (83), a linear regression of calculated ΔG_{diss} and experimental pK_a values accounted for systematic errors in the method:

$$pK_a = \frac{0.62}{RT \ln(10)} \Delta G_{diss} + 2.10 \quad (S4)$$

Unsurprisingly, the fit parameters in the ADF COSMO-RS implementation (0.62 and 2.10) are quite similar to those reported in Eckert et al. (83) for the continuum model (0.61 and 1.94). To account for the particular acetonitrile-water composition at which each analyte elutes from the LC column (the volume fraction of acetonitrile increases linearly from 12% at RT 3.00 to 62% at RT 7.50), a linear relationship developed by Espinosa et al. (84) was used to estimate analyte pK_a values in acetonitrile-water mixtures (${}^s pK_a$) of varying composition (0–60% v/v acetonitrile) from the corresponding aqueous pK_a values (${}^w pK_a$) calculated with COSMO-RS:

$${}^s pK_a = a_s {}^w pK_a + b_s \quad (S5)$$

As in the original expression, the IUPAC-recommended notation for pK_a and pH definitions is employed, wherein the solvent in which the properties are measured/calculated and the solvent referred to as the standard state, water (w) or acetonitrile-water (s), are indicated by left-hand superscripts and subscripts, respectively. Both the slope (a_s) and intercept (b_s) are related to differences in specific solvation interactions (e.g., hydrogen bonding) between water and the acetonitrile-water mixtures, and depend on the solute compound class. The intercept (b_s) is also related to differences in solvent basicities and dielectric constants. For specific values of a_s and b_s used in this study, see Equations 2 and 3 and Tables 4 and 5 in the original paper.

The pH of five acetonitrile-water mixtures ranging from 1 to 70% v/v acetonitrile were measured potentiometrically ($n = 3$) using a VWR Scientific 8015 pH meter, calibrated with certified aqueous buffers (pH 4.00 and 7.00, Fisher Scientific). Linear regression of the measured pH values as a function of the acetonitrile volume fraction ($R^2 > 0.995$) enabled calculation of the pH of the LC mobile phase at any point during the 12-min eluent program. The pH values obtained from this approach refer to water as the standard state (${}^w \text{pH}$). To convert from ${}^w \text{pH}$ to ${}^s \text{pH}$ (i.e., pH values that refer to the acetonitrile-water mixtures as the standard state), a conversion parameter (δ) derived by Espinosa et al. (85) was applied:

$$s_{\text{pH}} = {}_w\text{pH} + \delta \quad (\text{S6})$$

The δ term includes both the primary medium effect and the difference between the liquid-junction potentials of the electrode system in water and the acetonitrile-water mixtures. Specific values of δ used in this work were calculated from Equation 10 in the original paper. Given the estimated analyte s_{pK_a} and mobile phase s_{pH} values, the degree of ionization of each analyte (α) in the particular acetonitrile-water mobile phase at which it elutes from the LC column was calculated:

$$\alpha = \frac{10^{-s_{\text{pK}_a}}}{10^{-s_{\text{pK}_a}} + 10^{-s_{\text{pH}}}} \quad (\text{S7})$$

RIE values were determined for the five dimer esters with proposed molecular structures (Table S4), as well as for *cis*-pinic acid. For compounds with multiple sites for deprotonation (e.g., *cis*-pinic acid), *RIE* values were derived independently for each possible monoanion and the results were summed to give an aggregate *RIE*. *RIE* values were normalized to that of *cis*-pinic acid, and scaled by the measured *cis*-pinic acid (–)ESI efficiency. In this way, absolute (–)ESI efficiencies for the five dimer esters were ascertained. For the dimers with unknown molecular structures, (–)ESI efficiencies were approximated by those of the dimer esters with the most similar $\overline{\text{OS}}_{\text{C}}$ values (Table 1).

Due to fundamental differences in the (–)ESI behavior of monomers and oligomers, namely that larger molecules produce anions with more delocalized charge (lower *WAPS*), the theoretical (–)ESI efficiencies of the dimer esters are roughly an order of magnitude higher than that of *cis*-pinic acid (Table S4). These findings suggest that the mass contribution of oligomers to monoterpene SOA is significantly overestimated in studies that use commercially available terpenoic acids as surrogates to quantify oligomeric (–)ESI efficiencies (22, 23, 31, 76, 77). Indeed, dimers formed from coupled O_3 and OH oxidation (Table 1, types 1–3) are found to account for 25.4% of the total mass of β -pinene SOA formed after ~4 h of ozonolysis in the CTEC (Table S1, Exp. 1) when quantified using the measured (–)ESI efficiency of *cis*-pinic acid, whereas theoretical estimation of the (–)ESI efficiencies of the dimers via the model of Krueve et al. (78) leads to a mass fraction of only 5.9% for dimers produced via concerted O_3 and OH chemistry. The treatment

of oligomeric (–)ESI efficiencies in monoterpene SOA formation experiments, and its potential role as a source systematic bias, will be explored in detail in a forthcoming study on the abundance of oligomeric products in SOA derived from the O₃-initiated oxidation of α - and β -pinene.

S7.2 Uncertainty Analysis

Uncertainty in the PILS method (δ_{PILS}) arises mainly from variation in the collected liquid volume due to the existence of air bubbles, and has been estimated to be less than $\pm 11\%$ (47). Uncertainty associated with the chromatographic and mass spectral reproducibility of the UPLC/(–)ESI-Q-TOF-MS (δ_{UPLC}) was determined to be less than $\pm 3\%$ by performing replicate injections of a standard solution of adipic acid (99%, Sigma-Aldrich) and *cis*-pinonic acid (98%, Sigma-Aldrich). Uncertainty in the measured (–)ESI efficiency of *cis*-pinic acid ($\delta_{(-)\text{ESI}}$) was found to be small, less than $\pm 1\%$. An uncertainty of $\pm 20\%$ is assumed for SMPS-derived suspended SOA mass loadings (δ_{SMPS}) (86). For molecular products in β -pinene SOA quantified using *cis*-pinic acid, propagation of these individual uncertainties yields a total estimated relative uncertainty in the reported SOA mass fractions (δ_{total}) of $\pm 23\%$:

$$\begin{aligned}\delta_{\text{total}} &= \sqrt{\delta_{\text{PILS}}^2 + \delta_{\text{UPLC}}^2 + \delta_{(-)\text{ESI}}^2 + \delta_{\text{SMPS}}^2} \\ \delta_{\text{total}} &= \sqrt{(0.11)^2 + (0.03)^2 + (0.01)^2 + (0.20)^2} = 0.23\end{aligned}\quad (\text{S8})$$

For the mass fractions of dimeric compounds in O₃-derived β -pinene SOA quantified via the model of Krueve et al. (78), the most considerable contribution to the associated uncertainty arises from the error in the $\log RIE$ estimates. The root-mean-square deviation (RMSD) for the model validation set, a measure of the average disagreement between measured and predicted $\log RIE$ values, is taken as approximation of this error:

$$\text{RMSD} = \sqrt{\frac{\sum (\log RIE_{\text{p}} - \log RIE_{\text{m}})^2}{n}} \quad (\text{S9})$$

where $\log RIE_{\text{p}}$ and $\log RIE_{\text{m}}$ are the predicted and measured (–)ESI efficiencies relative to benzoic acid on a logarithmic scale, respectively, and n is the number of compounds in the model validation

set. The stated RMSD for the validation set is 0.48 log units (78), which translates to an estimated uncertainty in the reported SOA mass fractions of a factor of 3.

S8. General Applicability of O₃ + OH Oxidation to Monoterpene SOA Formation

Although specifically revealed in SOA formation from β -pinene, the production of dimers through concerted O₃ and OH oxidation is expected to be broadly applicable to other monoterpenes, most notably α -pinene. While the endocyclic double bond of α -pinene rules out the isotopic labeling approach that was used with β -pinene to directly probe this chemistry, several dimeric compounds with the accurate masses/molecular formulas corresponding to dimers demonstrated to derive from coupled O₃ and OH oxidation of β -pinene (Table 1, types 1–3) were measured by PILS + UPLC/(–)ESI-Q-TOF-MS in SOA produced from α -pinene ozonolysis (Table S5); two of the dimers, m/z 337 (C₁₉H₃₀O₅) and m/z 369 (C₁₉H₃₀O₇), are major peaks in the BPI chromatogram. These dimers were detected at either the same or similar RT (less than ± 0.18 min) to those of their β -pinene counterparts, and with analogous MS/MS spectra. The formation of these dimers was also significantly suppressed (>60%) by introduction of cyclohexane as an OH scavenger. These findings indirectly confirm that dimer production via synergistic O₃ + OH oxidation is operative in the α -pinene ozonolysis system. However, due to the structural isomerism of α - and β -pinene (i.e., endocyclic vs. exocyclic double bond), the scope of the O₃ + OH reactivity in the α -pinene system is likely underestimated by the limited number of equivalent/identical dimeric compounds formed via ozonolysis of α - and β -pinene reported in Table S5.

- (1) Schwantes RH, et al. (2017) Science of the Environmental Chamber. *Advances in Atmospheric Chemistry*, eds Barker JR, Steiner AL, Wallington TJ (World Scientific, Singapore), pp 1–93.
- (2) Loza CL, et al. (2014) Secondary organic aerosol yields of 12-carbon alkanes. *Atmos Chem Phys* 14:1423–1439.
- (3) Huang Y, et al. (2017) The Caltech Photooxidation Flow Tube reactor: design, fluid dynamics and characterization. *Atmos Meas Tech* 10:839–867.
- (4) Ma Y, Marston G (2008) Multifunctional acid formation from the gas-phase ozonolysis of β -pinene. *Phys Chem Chem Phys* 10:6115–6126.
- (5) Nguyen TL, Peeters J, Vereecken L (2009) Theoretical study of the gas-phase ozonolysis of β -pinene ($C_{10}H_{16}$). *Phys Chem Chem Phys* 11:5643–5656.
- (6) Eddingsaas NC, Loza CL, Yee LD, Seinfeld JH, Wennberg PO (2012) α -pinene photooxidation under controlled chemical conditions—Gas-phase composition in low- and high- NO_x environments. *Atmos Chem Phys* 12:6489–6504.
- (7) Bird RB, Stewart WE, Lightfoot EN (2007) *Transport Phenomena* (Wiley, New York), pp 546–549.
- (8) Keywood MD, et al. (2004) Secondary Organic Aerosol Formation from Cyclohexene Ozonolysis: Effect of OH Scavenger and the Role of Radical Chemistry. *Environ Sci Technol* 38:3343–3350.
- (9) Seinfeld JH, Pandis SN (2016) *Atmospheric Chemistry and Physics: From Air Pollution to Climate Change* (Wiley, Hoboken), pp 1098–1106.
- (10) Sipilä M, et al. (2014) Reactivity of stabilized Criegee intermediates (sCIs) from isoprene and monoterpene ozonolysis toward SO_2 and organic acids. *Atmos Chem Phys* 14:12143–12153.
- (11) Taatjes CA (2017) Criegee Intermediates: What Direct Production and Detection Can Teach Us About Reactions of Carbonyl Oxides. *Annu Rev Phys Chem* 68:183–207.
- (12) Anglada JM, Solé A (2016) Impact of water dimer on the atmospheric reactivity of carbonyl oxides. *Phys Chem Chem Phys* 18:17698–17712.
- (13) Shillings AJL, Ball SM, Barber MJ, Tennyson J, Jones RL (2011) An upper limit for water dimer absorption in the 750 nm spectral region and a revised water line list. *Atmos Chem Phys* 11:4273–4287.
- (14) Tolocka MP, et al. (2004) Formation of Oligomers in Secondary Organic Aerosol. *Environ Sci Technol* 38:1428–1434.
- (15) Wozniak AS, Bauer JE, Sleighter RL, Dickhut RM, Hatcher PG (2008) Technical Note: Molecular characterization of aerosol-derived water soluble organic carbon using ultrahigh resolution electrospray ionization Fourier transform ion cyclotron resonance mass spectrometry. *Atmos Chem Phys* 8:5099–5111.

- (16) Müller L, Reinnig MC, Hayen H, Hoffmann T (2009) Characterization of oligomeric compounds in secondary organic aerosol using liquid chromatography coupled to electrospray ionization Fourier transform ion cyclotron resonance mass spectrometry. *Rapid Commun Mass Spectrom* 23:971–979.
- (17) Gao Y, Hall WA, Johnston MV (2010) Molecular Composition of Monoterpene Secondary Organic Aerosol at Low Mass Loading. *Environ Sci Technol* 44:7897–7902.
- (18) Putman AL, et al. (2012) Ultrahigh-resolution FT-ICR mass spectrometry characterization of α -pinene ozonolysis SOA. *Atmos Environ* 46:164–172.
- (19) Witkowski B, Gierczak T (2014) Early stage composition of SOA produced by α -pinene/ozone reaction: α -Acyloxyhydroperoxy aldehydes and acidic dimers. *Atmos Environ* 95:59–70.
- (20) Kourtchev I, et al. (2015) Molecular composition of fresh and aged secondary organic aerosol from a mixture of biogenic volatile compounds: a high-resolution mass spectrometry study. *Atmos Chem Phys* 15:5683–5695.
- (21) Zhang X, et al. (2015) Formation and evolution of molecular products in α -pinene secondary organic aerosol. *Proc Natl Acad Sci USA* 112:14168–14173.
- (22) Kristensen K, et al. (2016) High-Molecular Weight Dimer Esters Are Major Products in Aerosols from α -Pinene Ozonolysis and the Boreal Forest. *Environ Sci Technol Lett* 3:280–285.
- (23) Kristensen K, Jensen LN, Glasius M, Bilde M (2017) The effect of sub-zero temperature on the formation and composition of secondary organic aerosol from ozonolysis of alpha-pinene. *Environ Sci: Processes Impacts* 19:1220–1234.
- (24) Mohr C, et al. (2017) Ambient observations of dimers from terpene oxidation in the gas phase: Implications for new particle formation and growth. *Geophys Res Lett* 44:2958–2966.
- (25) Sharpe SW, Sams RL, Johnson TJ (2002) The PNNL quantitative IR database for infrared remote sensing and hyperspectral imaging. *Proceedings of the 31st Applied Imagery Pattern Recognition Workshop*. DOI: 10.1109/aipr.2002.1182253.
- (26) Bahreini R, et al. (2005) Measurements of Secondary Organic Aerosol from Oxidation of Cycloalkenes, Terpenes, and *m*-Xylene Using an Aerodyne Aerosol Mass Spectrometer. *Environ Sci Technol* 39:5674–5688.
- (27) Malloy QGJ, et al. (2009) Real-Time Aerosol Density Determination Utilizing a Modified Scanning Mobility Particle Sizer–Aerosol Particle Mass Analyzer System. *Aerosol Sci Technol* 43:673–678.
- (28) Shilling JE, et al. (2009) Loading-dependent elemental composition of α -pinene SOA particle. *Atmos Chem Phys* 9:771–782.
- (29) Saathoff H, et al. (2009) Temperature dependence of yields of secondary organic aerosols from the ozonolysis of α -pinene and limonene. *Atmos Chem Phys* 9:1551–1577.

- (30) Kourtchev I, Copolovici L, Claeys M, Maenhaut W (2009) Characterization of Atmospheric Aerosols at a Forested Site in Central Europe. *Environ Sci Technol* 43:4665–4671.
- (31) Kristensen K, et al. (2013) Formation and occurrence of dimer esters of pinene oxidation products in atmospheric aerosols. *Atmos Chem Phys* 13:3763–3776.
- (32) Vogel AL, et al. (2013) In situ submicron organic aerosol characterization at a boreal forest research station during HUMPPA-COPEC 2010 using soft and hard ionization mass spectrometry. *Atmos Chem Phys* 13:10933–10950.
- (33) Vestenius M, et al. (2014) Acidic reaction products of monoterpenes and sesquiterpenes in atmospheric fine particles in a boreal forest. *Atmos Chem Phys* 14:7883–7893.
- (34) Isaacman-VanWertz G, et al. (2016). Ambient Gas-Particle Partitioning of Tracers for Biogenic Oxidation. *Environ Sci Technol* 50:9952–9962.
- (35) DeCarlo PF, et al. (2006) Field-Deployable, High-Resolution, Time-of-Flight Aerosol Mass Spectrometer. *Anal Chem* 78:8281–8289.
- (36) Allan JD, et al. (2004) A generalised method for the extraction of chemically resolved mass spectra from Aerodyne aerosol mass spectrometer data. *J Aerosol Sci* 35:909–922.
- (37) Aiken AC, et al. (2008) O/C and OM/OC Ratios of Primary, Secondary, and Ambient Organic Aerosols with High-Resolution Time-of-Flight Aerosol Mass Spectrometry. *Environ Sci Technol* 42:4478–4485.
- (38) Middlebrook AM, Bahreini R, Jimenez JL, Canagaratna MR (2012) Evaluation of Composition-Dependent Collection Efficiencies for the Aerodyne Aerosol Mass Spectrometer using Field Data. *Aerosol Sci Technol* 46:258–271.
- (39) Canagaratna MR, et al. (2015) Elemental ratio measurements of organic compounds using aerosol mass spectrometry: characterization, improved calibration, and implications. *Atmos Chem Phys* 15:253–272.
- (40) Chhabra PS, Flagan RC, Seinfeld JH (2010) Elemental analysis of chamber organic aerosol using an Aerodyne high-resolution aerosol mass spectrometer. *Atmos Chem Phys* 10:4111–4131.
- (41) Chen Q, Liu Y, Donahue NM, Shilling JE, Martin ST (2011) Particle-Phase Chemistry of Secondary Organic Material: Modeled Compared to Measured O:C and H:C Elemental Ratios Provide Constraints. *Environ Sci Technol* 45:4763–4770.
- (42) Donahue NM, et al. (2012) Aging of biogenic secondary organic aerosol via gas-phase OH radical reactions. *Proc Natl Acad Sci USA* 109:13503–13508.
- (43) Nakao S, et al. (2013) Density and elemental ratios of secondary organic aerosol: Application of a density prediction method. *Atmos Environ* 68:273–277.

- (44) Chhabra PS, et al. (2011) Elemental composition and oxidation of chamber organic aerosol. *Atmos Chem Phys* 11:8827–8845.
- (45) Weber RJ, et al. (2001) A Particle-into-Liquid Collector for Rapid Measurement of Aerosol Bulk Chemical Composition. *Aerosol Sci Technol* 35:718–727.
- (46) Sorooshian A, et al. (2006) Modeling and Characterization of a Particle-into-Liquid Sampler (PILS). *Aerosol Sci Technol* 40:396–409.
- (47) Zhang X, et al. (2016) Time-resolved molecular characterization of organic aerosols by PILS + UPLC/ESI-Q-TOFMS. *Atmos Environ* 130:180–189.
- (48) Mikuška P, Večeřa Z, Bartošíková A, Maenhaut W (2012) Annular diffusion denuder for simultaneous removal of gaseous organic compounds and air oxidants during sampling of carbonaceous aerosols. *Anal Chim Acta* 714:68–75.
- (49) Mutzel A, Rodigast M, Iinuma Y, Böge O, Herrmann H (2013) An improved method for the quantification of SOA bound peroxides. *Atmos Environ* 67:365–369.
- (50) CRC Press (2010) *CRC Handbook of Chemistry and Physics*, eds Haynes WM, Lide DR (CRC Press, Boca Raton), pp 8-42–8-51.
- (51) Nichols MA, Waner MJ (2010) Kinetic and Mechanistic Studies of the Deuterium Exchange in Classical Keto-Enol Tautomeric Equilibrium Reactions. *J Chem Educ* 87:952–955.
- (52) Zhao R, Kenseth CM, Huang Y, Dalleska NF, Seinfeld JH (2018) Iodometry-Assisted Liquid Chromatography Electrospray Ionization Mass Spectrometry for Analysis of Organic Peroxides: An Application to Atmospheric Secondary Organic Aerosol. *Environ Sci Technol* 52:2108–2117.
- (53) Docherty KS, Wu W, Lim YB, Ziemann PJ (2005) Contributions of Organic Peroxides to Secondary Organic Aerosol Formed from Reactions of Monoterpenes with O₃. *Environ Sci Technol* 39:4049–4059.
- (54) Jenkin ME (2004) Modelling the formation and composition of secondary organic aerosol from α - and β -pinene ozonolysis using MCM v3. *Atmos Chem Phys* 4:1741–1757.
- (55) Mertes P, Pfaffenberger L, Dommen J, Kalberer M, Baltensperger U (2012) Development of a sensitive long path absorption photometer to quantify peroxides in aerosol particles (Peroxide-LOPAP). *Atmos Meas Tech* 5:2339–2348.
- (56) Epstein SA, Blair SL, Nizkorodov SA (2014) Direct Photolysis of α -Pinene Ozonolysis Secondary Organic Aerosol: Effect on Particle Mass and Peroxide Content. *Environ Sci Technol* 48:11251–11258.
- (57) Li H, Chen Z, Huang L, Huang D (2016) Organic peroxides' gas-particle partitioning and rapid heterogeneous decomposition on secondary organic aerosol. *Atmos Chem Phys* 16:1837–1848.

- (58) Krapf M, et al. (2016) Labile Peroxides in Secondary Organic Aerosol. *Chem* 1:603–616.
- (59) Riva M, et al. (2017) Multiphase reactivity of gaseous hydroperoxide oligomers produced from isoprene ozonolysis in the presence of acidified aerosols. *Atmos Environ* 152:314–322.
- (60) Tong H, et al. (2016) Hydroxyl radicals from secondary organic aerosol decomposition in water. *Atmos Chem Phys* 16:1761–1771.
- (61) Wang Y, Kim H, Paulson SE (2011) Hydrogen peroxide generation from α - and β -pinene and toluene secondary organic aerosols. *Atmos Environ* 45:3149–3156.
- (62) Badali K, et al. (2015) Formation of hydroxyl radicals from photolysis of secondary organic aerosol material. *Atmos Chem Phys* 15:7831–7840.
- (63) Saunders SM, Jenkin ME, Derwent RG, Pilling MJ (2003) Protocol for the development of the Master Chemical Mechanism MCM v3 (Part A): tropospheric degradation of non-aromatic volatile organic compounds. *Atmos Chem Phys* 3:161–180.
- (64) Vereecken L, Peeters J (2012) A theoretical study of the OH-initiated gas-phase oxidation mechanism of β -pinene ($C_{10}H_{16}$): first generation products. *Phys Chem Chem Phys* 14:3802–3815.
- (65) Orlando JJ, Tyndall GS (2012) Laboratory studies of organic peroxy radical chemistry: an overview with emphasis on recent issues of atmospheric significance. *Chem Soc Rev* 41:6294–6317.
- (66) Yasmeen F, et al. (2010) Terpenylic acid and related compounds: precursors for dimers in secondary organic aerosol from the ozonolysis of α - and β -pinene. *Atmos Chem Phys* 10:9383–9392.
- (67) Yasmeen F, et al. (2011) Characterisation of tracers for aging in α -pinene secondary organic aerosol using liquid chromatography/negative ion electrospray ionisation mass spectrometry. *Environ Chem* 9:236–246.
- (68) Crounse JD, Nielsen LB, Jørgensen S, Kjaergaard HG, Wennberg PO (2013) Autoxidation of Organic Compounds in the Atmosphere. *J Phys Chem Lett* 4:3513–3520.
- (69) Ehn M, et al. (2014) A large source of low-volatility secondary organic aerosol. *Nature* 506:476–479.
- (70) Grossert JS, Fancy PD, White RL (2005) Fragmentation pathways of negative ions produced by electrospray ionization of acyclic dicarboxylic acids and derivatives. *Can J Chem* 83:1878–1890.
- (71) Demarque DP, Crotti AE, Vessecchi R, Lopes JL, Lopes, NP (2016) Fragmentation reactions using electrospray ionization mass spectrometry: an important tool for the structural elucidation and characterization of synthetic and natural products. *Nat Prod Rep* 33:432–455.
- (72) DePalma JW, Horan AJ, Hall WA, Johnston MV (2013) Thermodynamics of oligomer formation: Implications for secondary organic aerosol formation and reactivity. *Phys Chem Chem Phys* 15:6935–6944.

- (73) Yatavelli RLN, et al. (2014) Semicontinuous measurements of gas-particle partitioning of organic acids in a ponderosa pine forest using a MOVI-HRToF-CIMS. *Atmos Chem Phys* 14:1527–1546.
- (74) Donahue NM, Epstein SA, Pandis SN, Robinson AL (2011) A two-dimensional volatility basis set: 1. Organic-aerosol mixing thermodynamics. *Atmos Chem Phys* 11:3303–3318.
- (75) Konermann L, Ahadi E, Rodriguez AD, Vahidi S (2012) Unraveling the Mechanism of Electrospray Ionization. *Anal Chem* 85:2–9.
- (76) Kristensen K, et al. (2014) Dimers in α -pinene secondary organic aerosol: effect of hydroxyl radical, ozone, relative humidity and aerosol acidity. *Atmos Chem Phys* 14:4201–4218.
- (77) Sato K, et al. (2016) Terpenylic acid and nine-carbon multifunctional compounds formed during the aging of β -pinene ozonolysis secondary organic aerosol. *Atmos Environ* 130:127–135.
- (78) Krueve A, Kaupmees K, Liigand J, Leito I (2014) Negative Electrospray Ionization via Deprotonation: Predicting the Ionization Efficiency. *Anal Chem* 86:4822–4830.
- (79) Klamt A (1995) Conductor-like Screening Model for Real Solvents: A New Approach to the Quantitative Calculation of Solvation Phenomena. *J Phys Chem* 99:2224–2235.
- (80) Klamt A (2005) *COSMO-RS: From Quantum Chemistry to Fluid Phase Thermodynamics and Drug Design*. (Elsevier, Amsterdam).
- (81) Pye CC, Ziegler T, van Lenthe E, Louwen JN (2009) An implementation of the conductor-like screening model of solvation within the Amsterdam density functional package–Part II. COSMO for real solvents. *Can J Chem* 87:790–797.
- (82) Kaupmees K, Kaljurand I, Leito I (2010) Influence of Water Content on the Acidities in Acetonitrile, Quantifying Charge Delocalization in Anions. *J Phys Chem A* 114:11788–11793.
- (83) Eckert F, Diedenhofen M, Klamt A (2010) Towards a first principles prediction of pK_a : COSMO-RS and the cluster-continuum approach. *Mol Phys* 108:229–241.
- (84) Espinosa S, Bosch E, Rosés M (2002) Retention of ionizable compounds in high-performance liquid chromatography: 14. Acid-base pK values in acetonitrile-water mobile phases. *J Chromatogr A* 964:55–66.
- (85) Espinosa S, Bosch E, Rosés M (2000) Retention of Ionizable Compounds on HPLC. 5. pH Scales and the Retention of Acids and Bases with Acetonitrile-Water Mobile Phases. *Anal Chem* 72:5193–5200.
- (86) Ryerson TB, et al. (2013) The 2010 California Research at the Nexus of Air Quality and Climate Change (CalNex) field study. *J Geophys Res Atmos* 118:5830–5866.

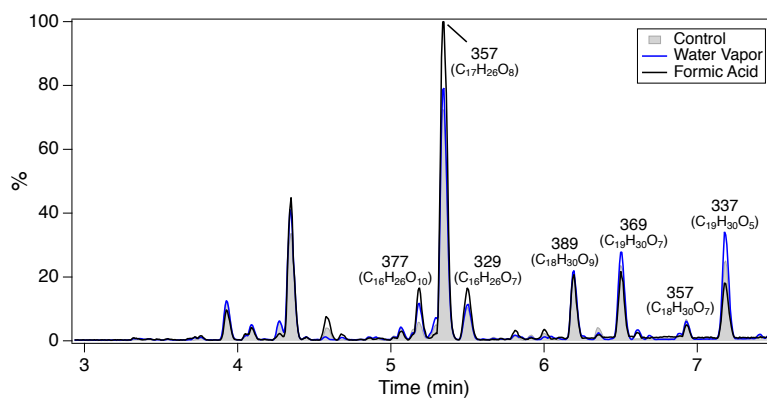


Fig. S1. UPLC/(-)ESI-Q-TOF-MS BPI chromatograms of SOA produced from the O_3 -initiated oxidation of β -pinene in the CPOT (Table S1, Exps. 7, 9, and 10) in the presence and absence of water vapor and formic acid as SCI scavengers (*SI Appendix*, S1.2). Numbers correspond to nominal m/z values of $[M-H]^-$ ions; molecular formulas are given in parentheses. Chromatograms for Control, Water Vapor, and Formic Acid experiments are normalized to the TOC content of the corresponding SOA samples (*SI Appendix*, S3.4) and are reported as averages of replicates ($n = 3$).

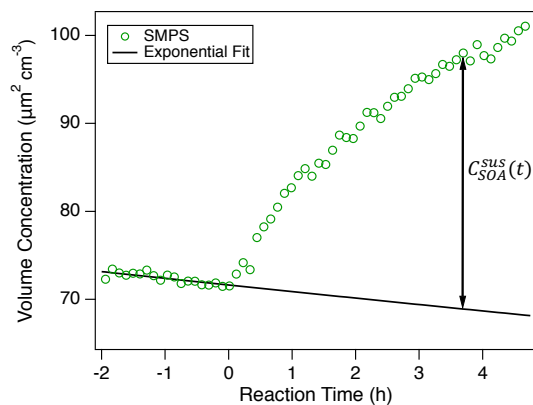


Fig. S2. Determination of SMPS-derived suspended SOA volume concentrations, $C_{SOA}^{SUS}(t)$. An exponential fit was applied to the decay of pure $(NH_4)_2SO_4$ seed ($t < 0$). The extrapolated seed volume concentrations ($t > 0$) were subtracted from the volume concentrations of total suspended aerosol measured by the SMPS. Data shown are for Exp. 1 in Table S1.

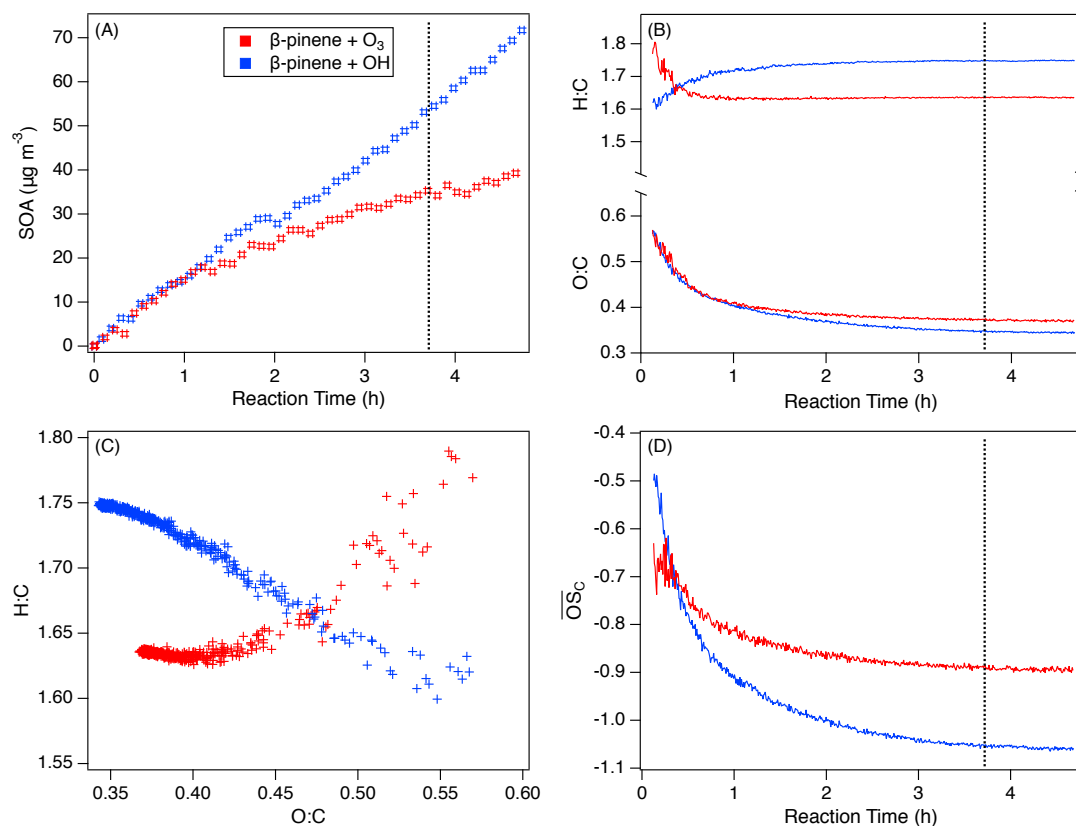


Fig. S3. “Bulk” properties of SOA produced from the O_3 - and OH-initiated oxidation of β -pinene over ~ 4 h of reaction in the CTEC (Table S1, Exps. 1 and 2). (A) SMPS-derived suspended SOA mass concentrations (*SI Appendix*, S3.1). (B) AMS-derived elemental O:C and H:C ratios (*SI Appendix*, S3.2). (C) van Krevelen diagram. (D) AMS-derived average carbon oxidation states ($\overline{\text{OS}}_{\text{C}} = 2 \text{ O:C} - \text{H:C}$). Dashed lines denote time point for which BPI chromatograms are presented in Fig. 1, SOA mass fractions are calculated in Table 1, and O:C, H:C, and $\overline{\text{OS}}_{\text{C}}$ values are reported in *SI Appendix*, S3.2.

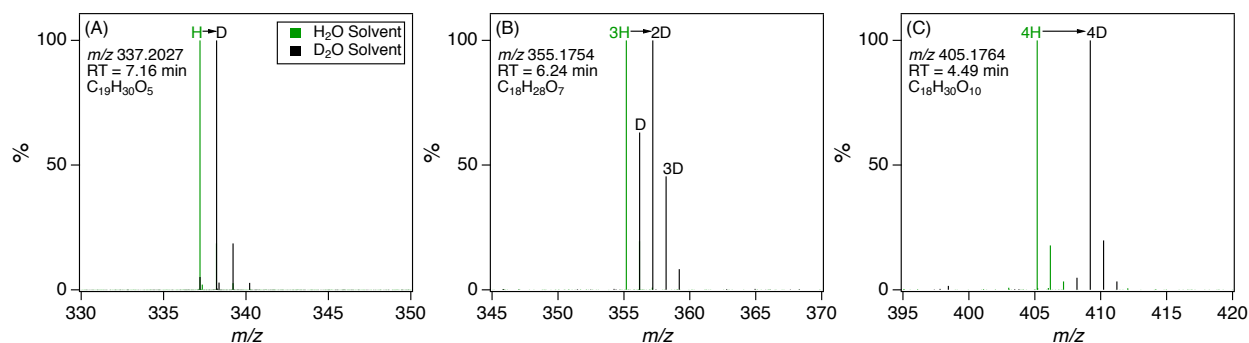


Fig. S4. Shift in m/z of representative dimers in β -pinene SOA, measured by UPLC/(-)ESI-Q-TOF-MS, due to H/D exchange of labile hydrogens (e.g., $-\text{OH}$, $-\text{OOH}$, and $-\text{COOH}$) when D_2O is used in place of H_2O as the solvent/polar eluent. The m/z shifts by one mass unit for every exchangeable hydrogen present in the molecule in addition to the site deprotonated to form the $[\text{M}-\text{H}]^-$ ion. The partial H/D exchange exemplified in B is attributed to structures containing moderately acidic α hydrogens (*SI Appendix*, S3.6).

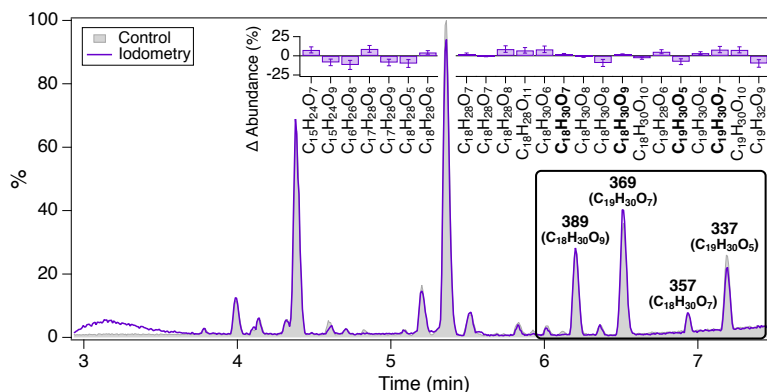


Fig. S5. UPLC/(-)ESI-Q-TOF-MS BPI chromatograms of SOA produced from the O_3 -initiated oxidation of β -pinene in the CPOT (Table S1, Exp. 7); comparison between iodometry and control samples (*SI Appendix*, S3.7). Numbers correspond to nominal m/z values of $[M-H]^-$ ions; molecular formulas are given in parentheses. (*Inset*) Effect of iodometry on the abundance of dimers whose formation was significantly inhibited ($>65\%$) by OH scavenging (Table 1), reported as a percent change relative to the control sample and precise to $<6\%$. Data for Control and Iodometry samples are reported as averages of replicates ($n = 3$).

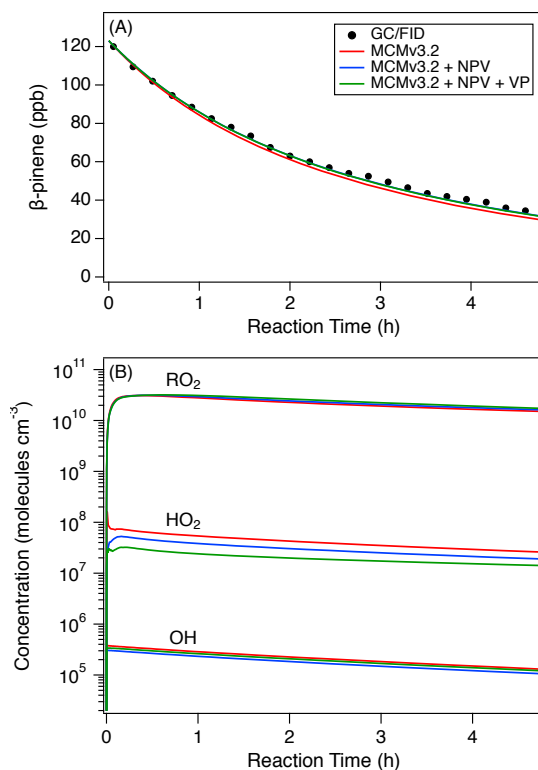


Fig. S6. MCMv3.2 simulations of the gas-phase ozonolysis of β -pinene in the CTEC under initial conditions of 123 ppb β -pinene, 200 ppb O_3 , zero NO_x , 295 K, 1 atm, and 5% RH (Table S1, Exp. 1). Three variations of the β -pinene ozonolysis mechanism were implemented (*SI Appendix*, S4). (A) First-order decay of β -pinene, measured by GC/FID and modeled. (B) Simulated concentration profiles of OH, HO_2 , and RO_2 .

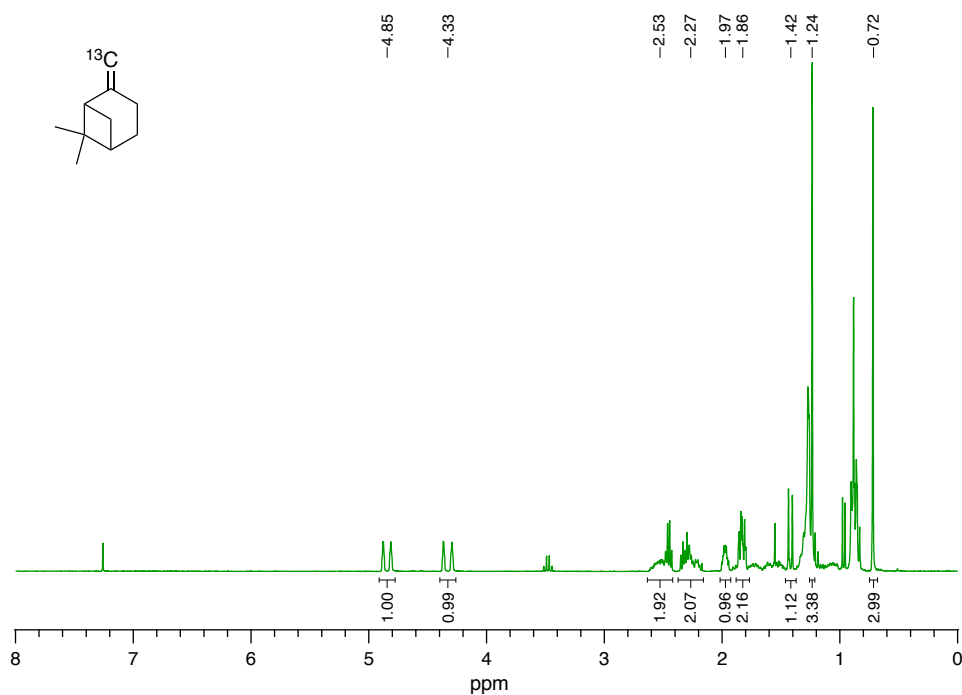


Fig. S7. ^1H NMR spectrum (300 MHz, CDCl_3) of ^{13}C - β -pinene.

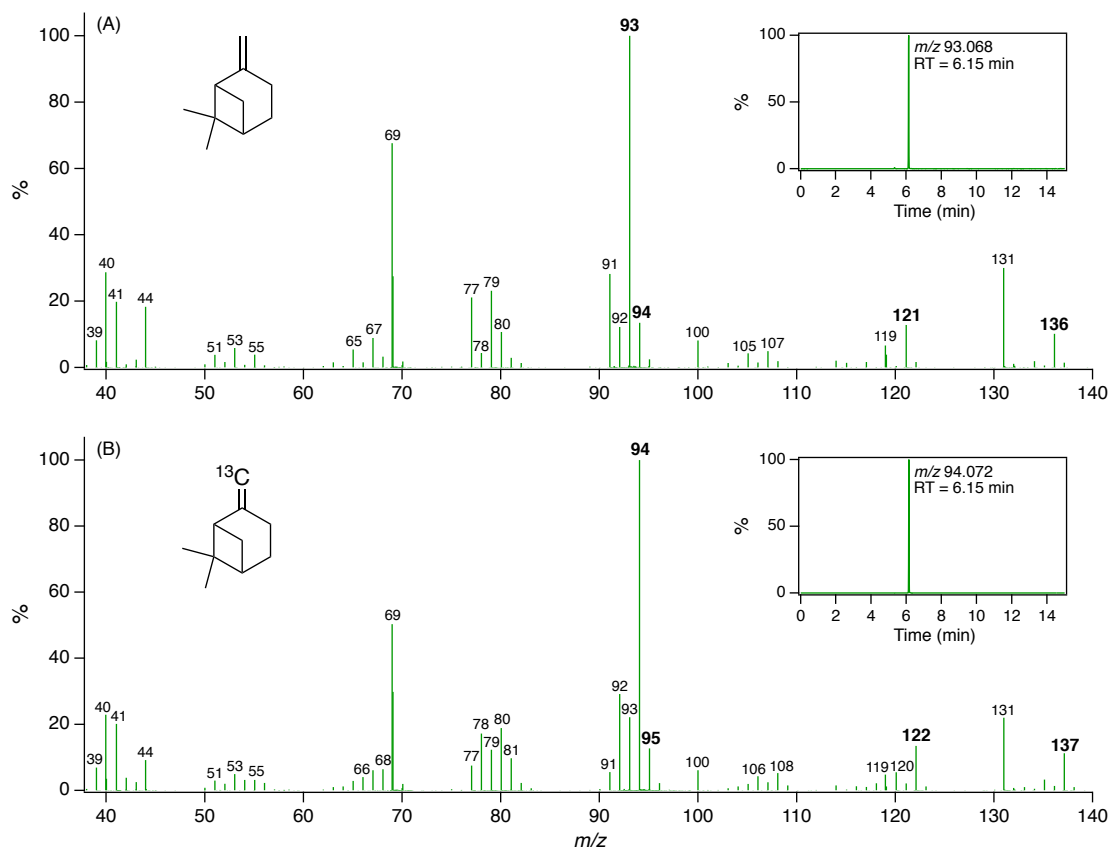


Fig. S8. GC/EI-MS spectra of (A) commercial β -pinene and (B) ^{13}C - β -pinene. (Insets) BPI chromatograms of A and B.

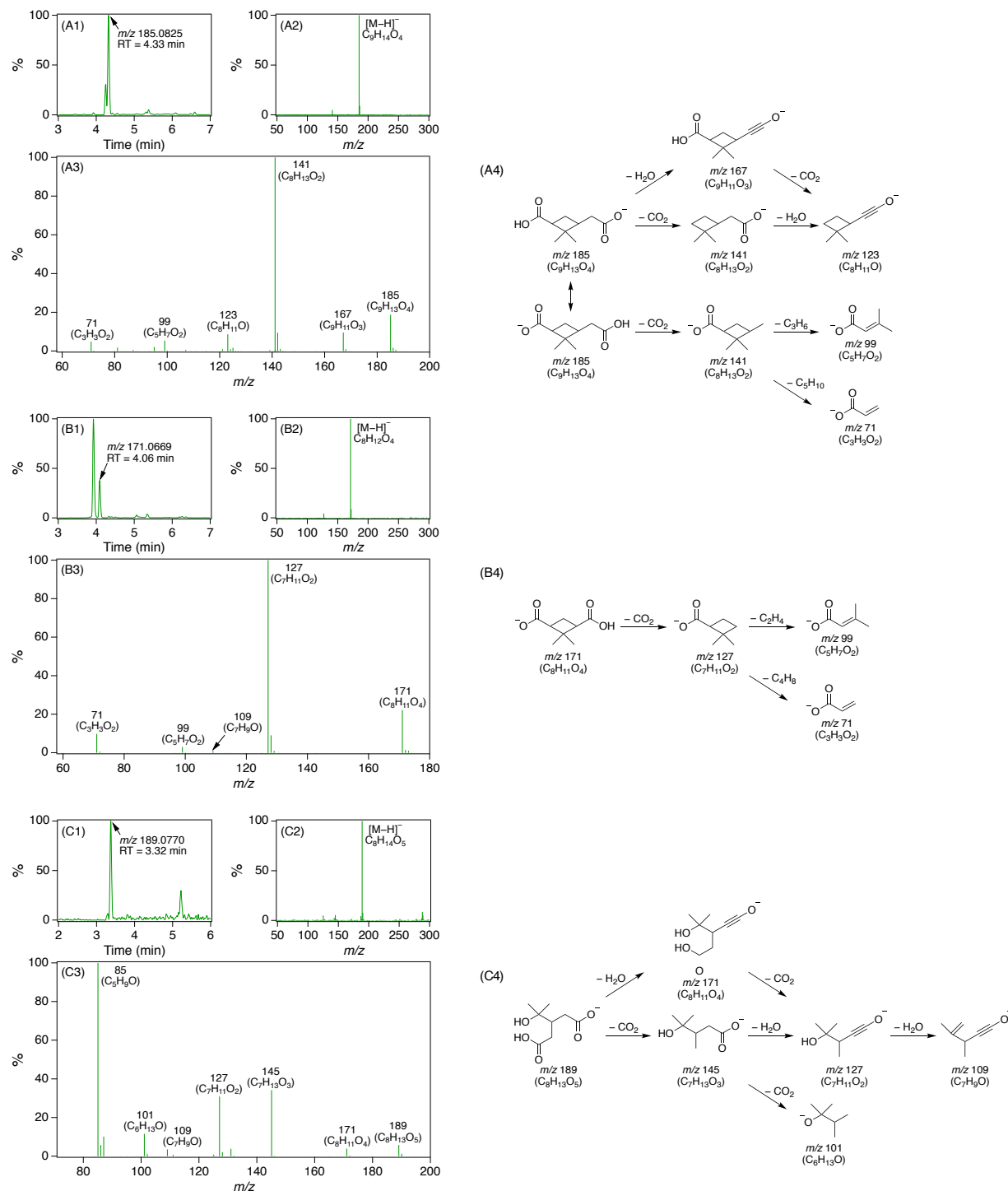


Fig. S9. (1) Extracted ion chromatograms, (2) MS spectra, and (3) MS/MS spectra, measured by UPLC/(–)ESI-Q-TOF-MS, along with (4) proposed fragmentation pathways, for dicarboxylic acids in β -pinene SOA assigned to (A) *cis*-pinic acid ($C_9H_{14}O_4$), (B) *cis*-norpinic acid ($C_8H_{12}O_4$), and (C) diaterpenylic acid ($C_8H_{14}O_5$). Numbers in MS/MS spectra and fragmentation pathways correspond to nominal m/z values of $[M-H]^-$ fragment ions; ionic formulas $[C_xH_yO_z]^-$ are given in parentheses.

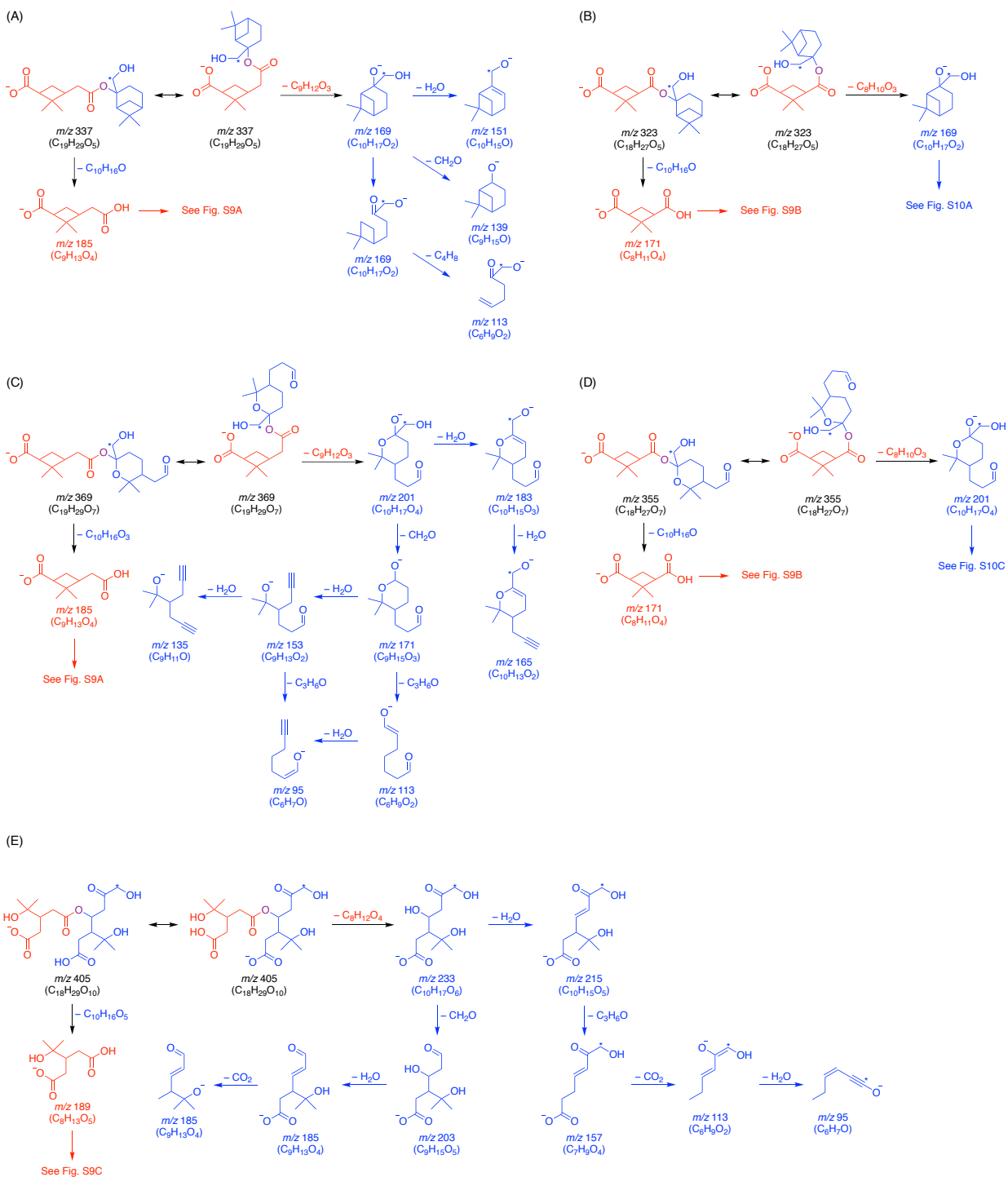


Fig. S10. Proposed fragmentation pathways for dimer esters (Table S4) formed from concerted O_3 and OH oxidation of β -pinene. Structures are colored to denote O_3 -derived (red) and OH-derived (blue) monomeric units. Numbers correspond to nominal m/z values of $[\text{M}-\text{H}]^-$ fragment ions; ionic formulas $[\text{C}_x\text{H}_y\text{O}_z]^-$ are given in parentheses. *Indicates position of ^{13}C label on formation from ^{13}C - β -pinene.

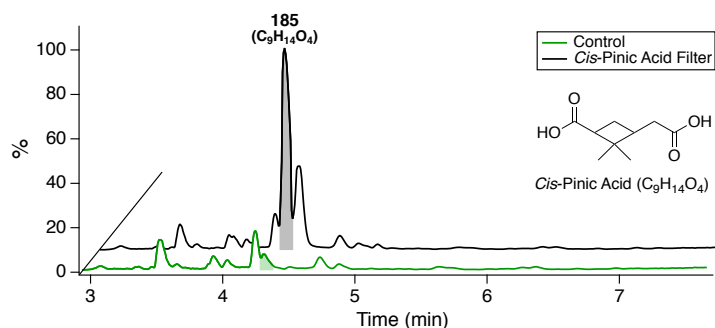


Fig. S11. UPLC/(-)ESI-Q-TOF-MS BPI chromatograms of SOA produced from the OH-initiated oxidation of β -pinene in the presence of pure $(\text{NH}_4)_2\text{SO}_4$ seed after ~ 4 h of reaction in the CTEC (Table S1, Exp. 5). SOA was collected on either a clean Teflon filter (Control) or a Teflon filter coated with *cis*-pinic acid ($\text{C}_9\text{H}_{14}\text{O}_4$). Filters were collected in parallel such that the mass of SOA on each filter was approximately equivalent (SI Appendix, S6.2). Shaded peaks correspond to *cis*-pinic acid.

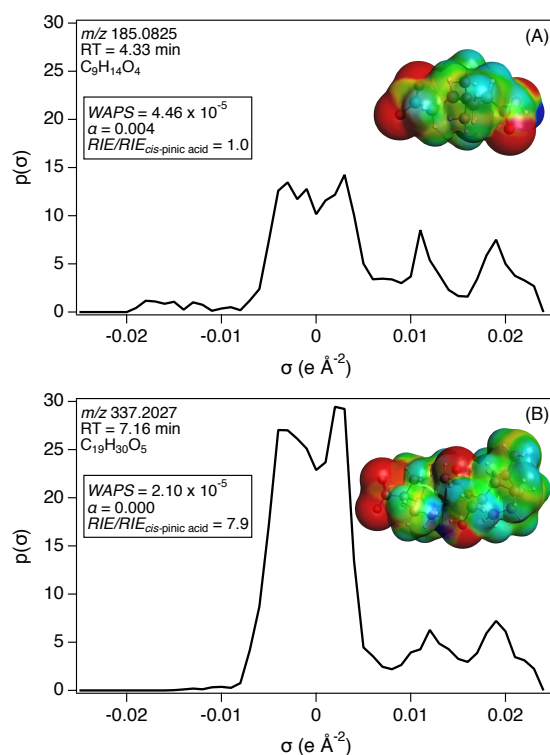


Fig. S12. COSMO-RS σ profiles of the $[\text{M}-\text{H}]^-$ ions of (A) *cis*-pinic acid ($\text{C}_9\text{H}_{14}\text{O}_4$) and (B) the dimer ester at m/z 337 ($\text{C}_{19}\text{H}_{30}\text{O}_5$). Each σ profile contains 90 segments, $0.0089 \text{ e } \text{\AA}^{-2}$ wide; positive σ values correspond to surface segments with negative charge. (Insets) COSMO surface charge density superposed on the ball-and-stick structure for each anion; red represents positive charge density (underlying molecular charge is negative), blue represents negative charge density (underlying molecular charge is positive). The calculated weighted average positive sigma (WAPS), degree of ionization in solution (α), and relative (-)ESI efficiency normalized to that of *cis*-pinic acid ($\text{RIE}/\text{RIE}_{\text{cis-pinic acid}}$) are also reported for each compound.

Table S1. Summary of experimental conditions.

Reactor	Exp.	VOC	[VOC] ₀ (ppb)	[O ₃] ₀ (ppb) [†]	Oxidant	Seed aerosol [‡]	Initial seed volume (μm ³ cm ⁻³)	OH/SCI scavenger	T ₀ (K)	RH ₀ (%)
Caltech 24 m ³ Environmental Chamber (CTEC)	1	β-pinene	123	~200	O ₃	(NH ₄) ₂ SO ₄	72	–	295 ± 2	<5
	2	β-pinene	117	~3	OH	(NH ₄) ₂ SO ₄	66	–	295 ± 2	<5
	3	β-pinene	124	~3	OH	(NH ₄) ₂ SO ₄ + <i>Cis</i> -Pinic Acid (1:1)	122	–	295 ± 2	<5
	4	β-pinene	132	~3	OH	(NH ₄) ₂ SO ₄ + <i>Cis</i> -Pinic Acid (2:1)	143	–	295 ± 2	<5
	5	β-pinene	127	~3	OH	(NH ₄) ₂ SO ₄	74	–	295 ± 2	<5
	6	α-pinene	124	~200	O ₃	(NH ₄) ₂ SO ₄	86	–	295 ± 2	<5
Caltech Photooxidation Flow Tube (CPOT)	7	β-pinene	147	~980	O ₃	(NH ₄) ₂ SO ₄	77	–	295 ± 2	<10
	8	β-pinene	149	~990	O ₃	(NH ₄) ₂ SO ₄	74	Cyclohexane (25 ppm)	295 ± 2	<10
	9	β-pinene	143	~1010	O ₃	(NH ₄) ₂ SO ₄	81	Formic Acid (15 ppm)	295 ± 2	<10
	10	β-pinene	146	~970	O ₃	(NH ₄) ₂ SO ₄	73	Water Vapor (1%)	295 ± 2	43 ± 1
	11	¹³ C-β-pinene	152	~990	O ₃	(NH ₄) ₂ SO ₄	79	–	295 ± 2	<10

[†]H₂O₂ interference artificially increases O₃ absorption monitor readout by ~2–3 ppb in photooxidation experiments.

[‡]Seed aerosol was dried and neutralized in all experiments.

Table S2. Laboratory and field observations of compounds with accurate masses/molecular formulas corresponding to the dimers identified in SOA produced from the O₃-initiated oxidation of β -pinene whose formation was significantly inhibited (>65%) by OH scavenging.

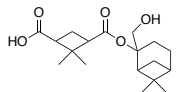
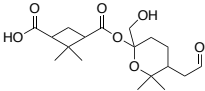
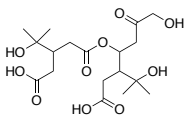
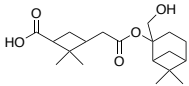
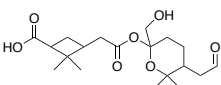
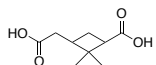
Dimer type	Observed <i>m/z</i> (–)	RT (min)	Molecular formula	Reported observations	
				Laboratory	Field
1	323.1860	6.86	C ₁₈ H ₂₈ O ₅	1,5	2
	355.1754	6.24	C ₁₈ H ₂₈ O ₇	3,5,8,9,10	2,9,11
	419.1525	4.70	C ₁₈ H ₂₈ O ₁₁	5	–
	373.1851	5.99	C ₁₈ H ₃₀ O ₈	5	11
	405.1764	4.49	C ₁₈ H ₃₀ O ₁₀	5,9,10	–
	351.1828	5.73	C ₁₉ H ₂₈ O ₆	1,5,10	11
	337.2027	7.16	C ₁₉ H ₃₀ O ₅	1,4,5,6,7,9,10	2,9
	369.1916	6.48	C ₁₉ H ₃₀ O ₇	3,5,7,9,10	2,9,11
2	341.1960	6.87	C ₁₈ H ₃₀ O ₆	–	11
	357.1919	6.91	C ₁₈ H ₃₀ O ₇	–	2
	373.1851	5.70	C ₁₈ H ₃₀ O ₈	5	11
	389.1814	6.18	C ₁₈ H ₃₀ O ₉	5	11
	353.1961	6.15	C ₁₉ H ₃₀ O ₆	5,9,10	9,11
3	315.1448	5.83	C ₁₅ H ₂₄ O ₇	5,9,10	9
	347.1346	5.19	C ₁₅ H ₂₄ O ₉	–	–
	375.1653	6.24	C ₁₇ H ₂₈ O ₉	5,6	11
	417.1769	6.76	C ₁₉ H ₃₀ O ₁₀	5	–
	403.1963	6.28	C ₁₉ H ₃₂ O ₉	5	–
4	345.1549	5.36	C ₁₆ H ₂₆ O ₈	5	11
	359.1714	5.89	C ₁₇ H ₂₈ O ₈	5,9,10	11
	339.1822	6.34	C ₁₈ H ₂₈ O ₆	3,5,9,10	2,11
	355.1754	5.27	C ₁₈ H ₂₈ O ₇	3,5,8,9,10	2,9,11
	371.1707	5.46	C ₁₈ H ₂₈ O ₈	3,5,9,10	9,11
(1) Tolocka et al. (14)			(7) Kourtchev et al. (20)		
(2) Wozniak et al. (15)			(8) Zhang et al. (21)		
(3) Müller et al. (16)			(9) Kristensen et al. (22)		
(4) Gao et al. (17)			(10) Kristensen et al. (23)		
(5) Putman et al. (18)			(11) Mohr et al. (24)		
(6) Witkowski and Gierczak (19)					

Table S3. MS/MS fragmentation patterns of dimers identified in SOA produced from the O₃-initiated oxidation of β -pinene whose m/z shifted by one mass unit on formation from ¹³C- β -pinene.

Dimer type	Observed m/z (-)	RT (min)	Molecular formula	Major MS/MS fragment ions [†]
1	323.1860	6.86	C ₁₈ H ₂₈ O ₅	¹⁷¹ (C ₈ H ₁₁ O ₄), ¹²⁷ (C ₇ H ₁₁ O ₂), ⁹⁹ (C ₅ H ₇ O ₂), ⁷¹ (C ₃ H ₃ O ₂) ¹⁶⁹ *(C ₁₀ H ₁₇ O ₂), ¹⁵¹ *(C ₁₀ H ₁₅ O), ¹³⁹ (C ₉ H ₁₅ O), ¹¹³ *(C ₆ H ₉ O ₂)
	355.1754	6.24	C ₁₈ H ₂₈ O ₇	³²⁵ (C ₁₇ H ₂₅ O ₆) ¹⁷¹ (C ₈ H ₁₁ O ₄), ¹²⁷ (C ₇ H ₁₁ O ₂), ⁹⁹ (C ₅ H ₇ O ₂), ⁷¹ (C ₃ H ₃ O ₂) ²⁰¹ *(C ₁₀ H ₁₇ O ₄), ¹⁸³ *(C ₁₀ H ₁₅ O ₃), ¹⁷¹ (C ₉ H ₁₅ O ₃), ¹⁵³ (C ₉ H ₁₃ O ₂), ¹³⁵ (C ₉ H ₁₁ O), ¹¹³ (C ₆ H ₉ O ₂), ⁹⁵ (C ₆ H ₇ O)
	419.1525	4.70	C ₁₈ H ₂₈ O ₁₁	³⁴³ (C ₁₆ H ₂₃ O ₈) ¹⁸⁹ (C ₈ H ₁₃ O ₅), ¹⁷¹ (C ₈ H ₁₁ O ₄), ¹⁴⁵ (C ₇ H ₁₃ O ₃), ¹²⁷ (C ₇ H ₁₁ O ₂), ¹⁰⁹ (C ₇ H ₉ O), ⁸⁵ (C ₅ H ₉ O) ²⁴⁷ *(C ₁₀ H ₁₅ O ₇), ²⁰³ (C ₉ H ₁₅ O ₅), ¹⁸⁵ (C ₉ H ₁₃ O ₄), ¹⁷¹ (C ₈ H ₁₁ O ₄), ¹⁴¹ (C ₈ H ₁₃ O ₂), ⁷⁵ *(C ₂ H ₃ O ₃)
	373.1851	5.99	C ₁₈ H ₃₀ O ₈	³⁴³ (C ₁₇ H ₂₇ O ₇), ³²⁵ (C ₁₇ H ₂₅ O ₆), ²⁹⁹ (C ₁₆ H ₂₇ O ₅), ²⁸¹ (C ₁₆ H ₂₅ O ₄) ¹⁸⁹ (C ₈ H ₁₃ O ₅), ¹⁷¹ (C ₈ H ₁₁ O ₄), ¹⁴⁵ (C ₇ H ₁₃ O ₃), ¹²⁷ (C ₇ H ₁₁ O ₂), ¹⁰⁹ (C ₇ H ₉ O), ⁸⁵ (C ₅ H ₉ O) ¹⁷¹ (C ₉ H ₁₅ O ₃), ¹³⁵ (C ₉ H ₁₁ O), ¹¹³ (C ₆ H ₉ O ₂), ⁹⁵ (C ₆ H ₇ O)
	405.1764	4.49	C ₁₈ H ₃₀ O ₁₀	¹⁸⁹ (C ₈ H ₁₃ O ₅), ¹⁷¹ (C ₈ H ₁₁ O ₄), ¹⁴⁵ (C ₇ H ₁₃ O ₃), ¹²⁷ (C ₇ H ₁₁ O ₂), ¹⁰⁹ (C ₇ H ₉ O), ⁸⁵ (C ₅ H ₉ O) ²³³ *(C ₁₀ H ₁₇ O ₆), ²¹⁵ *(C ₁₀ H ₁₅ O ₅), ²⁰³ (C ₉ H ₁₅ O ₅), ¹⁸⁵ (C ₉ H ₁₃ O ₄), ¹⁵⁷ *(C ₇ H ₉ O ₄), ¹⁴¹ (C ₈ H ₁₃ O ₂), ¹¹³ *(C ₆ H ₉ O ₂), ⁹⁵ *(C ₆ H ₇ O)
	351.1828	5.73	C ₁₉ H ₂₈ O ₆	¹⁸⁵ (C ₉ H ₁₃ O ₄), ¹⁶⁷ (C ₉ H ₁₁ O ₃), ¹⁴¹ (C ₈ H ₁₃ O ₂), ¹²³ (C ₈ H ₁₁ O), ⁹⁹ (C ₅ H ₇ O ₂), ⁷¹ (C ₃ H ₃ O ₂) ¹⁸³ *(C ₁₀ H ₁₅ O ₃), ¹⁶⁵ *(C ₁₀ H ₁₃ O ₂), ¹⁵³ (C ₉ H ₁₃ O ₂), ¹³⁵ (C ₉ H ₁₁ O)
	337.2027	7.16	C ₁₉ H ₃₀ O ₅	¹⁸⁵ (C ₉ H ₁₃ O ₄), ¹⁶⁷ (C ₉ H ₁₁ O ₃), ¹⁴¹ (C ₈ H ₁₃ O ₂), ¹²³ (C ₈ H ₁₁ O), ⁹⁹ (C ₅ H ₇ O ₂), ⁷¹ (C ₃ H ₃ O ₂) ¹⁶⁹ *(C ₁₀ H ₁₇ O ₂), ¹⁵¹ *(C ₁₀ H ₁₅ O), ¹³⁹ (C ₉ H ₁₅ O), ¹¹³ *(C ₆ H ₉ O ₂)
	369.1916	6.48	C ₁₉ H ₃₀ O ₇	³³⁹ (C ₁₈ H ₂₇ O ₆), ³²¹ (C ₁₈ H ₂₅ O ₅) ¹⁸⁵ (C ₉ H ₁₃ O ₄), ¹⁶⁷ (C ₉ H ₁₁ O ₃), ¹⁴¹ (C ₈ H ₁₃ O ₂), ¹²³ (C ₈ H ₁₁ O), ⁹⁹ (C ₅ H ₇ O ₂), ⁷¹ (C ₃ H ₃ O ₂) ²⁰¹ *(C ₁₀ H ₁₇ O ₄), ¹⁸³ *(C ₁₀ H ₁₅ O ₃), ¹⁷¹ (C ₉ H ₁₅ O ₃), ¹⁶⁵ *(C ₁₀ H ₁₃ O ₂), ¹⁵³ (C ₉ H ₁₃ O ₂), ¹³⁵ (C ₉ H ₁₁ O), ¹¹³ (C ₆ H ₉ O ₂), ⁹⁵ (C ₆ H ₇ O)
	341.1960	6.87	C ₁₈ H ₃₀ O ₆	³¹¹ (C ₁₇ H ₂₇ O ₅), ²⁵³ (C ₁₄ H ₂₁ O ₄) ¹⁵⁷ (C ₈ H ₁₃ O ₃), ¹³⁹ (C ₈ H ₁₁ O ₂), ¹⁸³ *(C ₁₀ H ₁₅ O ₃), ¹⁷¹ (C ₉ H ₁₅ O ₃), ¹⁶⁵ *(C ₁₀ H ₁₃ O ₂), ¹²⁵ *(C ₇ H ₉ O ₂), ¹¹³ (C ₆ H ₉ O ₂), ¹⁰⁷ *(C ₇ H ₇ O), ⁹⁵ (C ₆ H ₇ O), ⁷³ *(C ₃ H ₅ O ₂)
	357.1919	6.91	C ₁₈ H ₃₀ O ₇	³¹¹ (C ₁₇ H ₂₇ O ₅), ²⁵⁵ *(C ₁₄ H ₂₃ O ₄) ¹⁸⁹ (C ₈ H ₁₃ O ₅), ¹⁷³ (C ₇ H ₉ O ₅), ¹⁷¹ (C ₈ H ₁₁ O ₄), ¹⁴⁵ (C ₇ H ₁₃ O ₃), ¹³⁰ (C ₅ H ₆ O ₄), ¹²⁷ (C ₇ H ₁₁ O ₂), ¹⁰¹ (C ₆ H ₁₃ O), ⁸⁵ (C ₅ H ₉ O) ¹⁶⁹ *(C ₁₀ H ₁₇ O ₂), ¹⁵¹ *(C ₁₀ H ₁₅ O), ¹³⁹ *(C ₉ H ₁₅ O), ¹¹⁷ *(C ₅ H ₉ O ₃), ⁹⁹ *(C ₅ H ₇ O ₂), ⁷¹ *(C ₄ H ₇ O)
2	373.1851	5.70	C ₁₈ H ₃₀ O ₈	³⁴³ (C ₁₇ H ₂₇ O ₇) ¹⁸⁹ (C ₈ H ₁₃ O ₅), ¹⁷¹ (C ₈ H ₁₁ O ₄), ¹⁴⁵ (C ₇ H ₁₃ O ₃), ¹³¹ (C ₅ H ₇ O ₄), ¹²⁷ (C ₇ H ₁₁ O ₂), ¹⁰⁹ (C ₇ H ₉ O), ⁸⁷ (C ₄ H ₇ O ₂) ¹⁸⁵ (C ₉ H ₁₃ O ₄), ¹⁶⁷ (C ₉ H ₁₁ O ₃), ¹⁴¹ (C ₈ H ₁₃ O ₂), ¹²³ (C ₈ H ₁₁ O)
	389.1814	6.18	C ₁₈ H ₃₀ O ₉	¹⁸⁹ (C ₈ H ₁₃ O ₅), ¹⁷³ (C ₇ H ₉ O ₅), ¹⁷¹ (C ₈ H ₁₁ O ₄), ¹⁴⁵ (C ₇ H ₁₃ O ₃), ¹³⁰ (C ₅ H ₆ O ₄), ¹²⁷ (C ₇ H ₁₁ O ₂), ¹⁰¹ (C ₆ H ₁₃ O), ⁸⁵ (C ₅ H ₉ O) ¹⁷¹ (C ₉ H ₁₅ O ₃), ¹⁶⁵ *(C ₁₀ H ₁₃ O ₂), ¹²⁵ *(C ₇ H ₉ O ₂), ¹¹⁷ *(C ₅ H ₉ O ₃), ¹⁰⁷ *(C ₇ H ₇ O), ⁹⁹ *(C ₅ H ₇ O ₂), ⁹⁵ (C ₆ H ₇ O), ⁷¹ *(C ₄ H ₇ O)
	353.1961	6.15	C ₁₉ H ₃₀ O ₆	¹⁸⁵ (C ₉ H ₁₃ O ₄), ¹⁶⁷ (C ₉ H ₁₁ O ₃), ¹⁴¹ (C ₈ H ₁₃ O ₂), ¹²³ (C ₈ H ₁₁ O), ⁹⁹ (C ₅ H ₇ O ₂), ⁷¹ (C ₃ H ₃ O ₂) ¹⁸⁵ *(C ₁₀ H ₁₇ O ₃), ¹⁸³ *(C ₁₀ H ₁₅ O ₃), ¹⁵⁵ *(C ₉ H ₁₅ O ₂), ¹⁵³ *(C ₉ H ₁₃ O ₂), ⁸⁵ *(C ₄ H ₅ O ₂), ⁷³ *(C ₃ H ₅ O ₂)
	315.1448	5.83	C ₁₅ H ₂₄ O ₇	¹⁴⁵ (C ₅ H ₅ O ₅), ¹⁰¹ (C ₄ H ₅ O ₃), ⁸³ (C ₄ H ₃ O ₂), ⁵⁷ (C ₃ H ₅ O) ¹⁶⁹ *(C ₁₀ H ₁₇ O ₂), ¹⁵¹ *(C ₁₀ H ₁₅ O), ¹³⁹ (C ₉ H ₁₅ O)
	347.1346	5.19	C ₁₅ H ₂₄ O ₉	¹⁸⁹ (C ₈ H ₁₃ O ₅), ¹⁷¹ (C ₈ H ₁₁ O ₄), ¹⁴⁵ (C ₇ H ₁₃ O ₃), ¹²⁷ (C ₇ H ₁₁ O ₂), ¹⁰⁹ (C ₇ H ₉ O), ⁸⁵ (C ₅ H ₉ O) ¹²⁵ *(C ₇ H ₉ O ₂), ¹⁰⁷ *(C ₇ H ₇ O), ¹⁰¹ (C ₄ H ₅ O ₃), ⁸³ (C ₄ H ₃ O ₂), ⁵⁷ (C ₃ H ₅ O)
3	375.1653	6.24	C ₁₇ H ₂₈ O ₉	¹⁷⁵ (C ₇ H ₁₁ O ₅), ¹⁷³ (C ₇ H ₉ O ₅), ¹⁵⁷ (C ₇ H ₉ O ₄), ¹²⁹ (C ₆ H ₉ O ₃), ¹¹⁷ (C ₄ H ₅ O ₄), ⁹⁹ (C ₄ H ₃ O ₃), ⁸⁵ (C ₅ H ₉ O), ⁷³ (C ₃ H ₅ O ₂) ¹⁷¹ (C ₉ H ₁₅ O ₃), ¹⁶⁵ *(C ₁₀ H ₁₃ O ₂), ¹³⁵ *(C ₉ H ₁₁ O), ¹²⁵ *(C ₇ H ₉ O ₂), ¹¹³ (C ₆ H ₉ O ₂), ¹⁰⁷ *(C ₇ H ₇ O), ⁹⁵ (C ₆ H ₇ O)
	417.1769	6.76	C ₁₉ H ₃₀ O ₁₀	¹⁸⁹ (C ₈ H ₁₃ O ₅), ¹⁷³ (C ₇ H ₉ O ₅), ¹⁷¹ (C ₈ H ₁₁ O ₄), ¹⁴⁵ (C ₇ H ₁₃ O ₃), ¹³⁰ (C ₅ H ₆ O ₄), ¹²⁷ (C ₇ H ₁₁ O ₂), ¹⁰¹ (C ₆ H ₁₃ O), ⁸⁵ (C ₅ H ₉ O) ¹⁷¹ (C ₉ H ₁₅ O ₃), ¹⁶⁵ *(C ₁₀ H ₁₃ O ₂), ¹²⁵ *(C ₇ H ₉ O ₂), ¹⁰⁷ *(C ₇ H ₇ O), ⁹⁵ (C ₆ H ₇ O),
	403.1963	6.28	C ₁₉ H ₃₂ O ₉	²⁰³ (C ₉ H ₁₅ O ₅), ¹⁸⁵ (C ₉ H ₁₃ O ₄), ¹⁵⁹ (C ₈ H ₁₅ O ₃), ¹⁴¹ (C ₈ H ₁₃ O ₂), ¹²³ (C ₈ H ₁₁ O), ¹¹⁵ (C ₇ H ₁₅ O), ⁹⁹ (C ₆ H ₁₁ O) ¹⁷¹ (C ₉ H ₁₅ O ₃), ¹²⁵ *(C ₇ H ₉ O ₂), ¹¹³ *(C ₆ H ₉ O ₂), ¹⁰⁷ *(C ₇ H ₇ O), ⁹⁵ *(C ₆ H ₇ O), ⁸⁵ *(C ₅ H ₉ O)

[†]Nominal m/z values are colored to denote O₃-derived (red) and OH-derived (blue) fragment ions. Ionic formulas [C_xH_yO_z]⁺ are given in parentheses. *Indicates peaks that underwent a one-unit mass shift on formation from ¹³C- β -pinene.

Table S4. COSMO-RS theoretical parameters for proposed molecular structures of dimer esters (Table 1, type 1) formed from concerted O₃ and OH oxidation of β -pinene, and for *cis*-pinic acid.

Observed <i>m/z</i> (–)	RT (min)	Molecular formula	Exchangeable hydrogens	WAPS ($\times 10^5$) [†]	α^{\ddagger}	RIE/ RIE _{<i>cis</i>-pinic acid} [§]	Proposed molecular structure
323.1860	6.86	C ₁₈ H ₂₈ O ₅	2	2.18	0.005	7.3	
355.1754	6.24	C ₁₈ H ₂₈ O ₇	4	2.35	0.018	6.4	
405.1764	4.49	C ₁₈ H ₃₀ O ₁₀	5	2.18 2.17	0.099 0.055	21.5	
337.2027	7.16	C ₁₉ H ₃₀ O ₅	2	2.10	0.001	7.9	
369.1916	6.48	C ₁₉ H ₃₀ O ₇	4	2.25	0.045	8.3	
185.0825	4.33	C ₉ H ₁₄ O ₄	2	4.47 4.46	0.004 0.008	1.0	

[†]Weighted average positive sigma. [‡]Degree of ionization in solution. [§]Relative (–)ESI efficiency normalized to that of *cis*-pinic acid.

Table S5. Dimers identified in SOA produced from the O₃-initiated oxidation of α -pinene (Table S1, Exp. 6) with the same accurate masses/molecular formulas, similar RT, and analogous MS/MS spectra to those in β -pinene SOA demonstrated to derive from concerted O₃ and OH oxidation.

Dimer type	Observed <i>m/z</i> (–)	RT (min)		Molecular formula	Error (ppm)
		α -pinene	β -pinene		
1	323.1860	6.93	6.86	C ₁₈ H ₂₈ O ₅	0.6
	323.1860	6.68	6.86	C ₁₈ H ₂₈ O ₅	0.6
	337.2027	7.31	7.16	C ₁₉ H ₃₀ O ₅	3.6
	369.1916	6.48	6.48	C ₁₉ H ₃₀ O ₇	0.8
2	357.1919	6.91	6.91	C ₁₈ H ₃₀ O ₇	1.7
	357.1919	6.77	6.91	C ₁₈ H ₃₀ O ₇	1.7
	389.1814	6.02	6.18	C ₁₈ H ₃₀ O ₉	0.8
	353.1961	6.31	6.15	C ₁₉ H ₃₀ O ₆	–0.8